

1 Large fresh water influx induced salinity gradient and diagenetic 2 changes in the northern Indian Ocean dominate the stable oxygen 3 isotopic variation in *Globigerinoides ruber* 4

5 Rajeev Saraswat^{1*}, Thejasino Suokhrie¹, Dinesh K. Naik², Dharmendra P. Singh³, Syed M.
6 Saalim⁴, Mohd Salman^{1,5}, Gavendra Kumar^{1,5}, Sudhira R. Bhadra¹, Mahyar Mohtadi⁶, Sujata R.
7 Kurtarkar¹, Abhayanand S. Maurya³

8 ¹ Micropaleontology Laboratory, National Institute of Oceanography, Goa, India

9 ² Banaras Hindu University, Varanasi, Uttar Pradesh, India

10 ³ Indian Institute of Technology, Roorkee, India

11 ⁴ National Center for Polar and Ocean Research, Goa, India

12 ⁵ School of Earth, Ocean and Atmospheric Sciences, Goa University, Goa

13 ⁶ MARUM, University of Bremen, Bremen, Germany

14 * Correspondence to: Rajeev Saraswat (rsaraswat@nio.org)

15
16 **Abstract.** The application of stable oxygen isotopic ratio of surface dwelling *Globigerinoides ruber* (white variety)
17 ($\delta^{18}\text{O}_{ruber}$) to reconstruct past hydrological changes requires precise understanding of the effect of ambient parameters
18 on $\delta^{18}\text{O}_{ruber}$. The northern Indian Ocean, with huge freshwater influx and being a part of the Indo-Pacific Warm Pool,
19 provides a unique setting to understand the effect of both the salinity and temperature on $\delta^{18}\text{O}_{ruber}$. Here, we use a total
20 of 400 surface samples (252 from this work and 148 from previous studies), covering the entire salinity end member
21 region, to assess the effect of **fresh water influx induced seawater salinity** and temperature on $\delta^{18}\text{O}_{ruber}$ in the northern
22 Indian Ocean. The analyzed surface $\delta^{18}\text{O}_{ruber}$ very well mimics the expected $\delta^{18}\text{O}$ calcite estimated from the modern
23 seawater parameters (temperature, salinity and seawater $\delta^{18}\text{O}$). We report a large diagenetic overprinting of $\delta^{18}\text{O}_{ruber}$
24 in the surface sediments with an increase of 0.18‰ per kilometer increase in water depth. The **fresh water influx**
25 **induced salinity** exerts the major control on $\delta^{18}\text{O}_{ruber}$ ($R^2 = 0.63$) in the northern Indian Ocean, with an increase of
26 0.29‰ per unit increase in salinity. The relationship between temperature and salinity corrected $\delta^{18}\text{O}_{ruber}$ ($\delta^{18}\text{O}_{ruber} -$
27 $\delta^{18}\text{O}_{sw}$) in the northern Indian Ocean [$T = -0.59 * (\delta^{18}\text{O}_{ruber} - \delta^{18}\text{O}_{sw}) + 26.40$] is different than reported previously based
28 on the global compilation of plankton tow $\delta^{18}\text{O}_{ruber}$ data. The revised equations will help in better paleoclimatic
29 reconstruction from the northern Indian Ocean.
30

31 1. Introduction

32 The stable oxygen isotopic ratio ($\delta^{18}\text{O}$) of biogenic carbonates is one of the most extensively used marine paleoclimatic
33 proxies (Mulitza et al., 1997; Lea, 2014; Metcalfe et al., 2019; Saraswat et al., 2019). Even though it was initially
34 suggested that the oxygen isotopic fractionation in biogenic carbonates is largely driven by temperature (Urey et al.,
35 1947), subsequent work revealed that besides temperature, salinity and carbonate ion concentration of ambient
36 seawater also affect the biogenic carbonate $\delta^{18}\text{O}$ (Vergnaud-Grazzini, 1976; Spero et al., 1997; Bemis et al., 1998;
37 Spero et al., 1997; Bijma et al., 1999; Mulitza et al., 2003). On longer time-scales, the global ice volume contributes
38 the largest fraction ($\sim 1.0\text{-}1.2\%$) of the glacial-interglacial shift in marine biogenic carbonate $\delta^{18}\text{O}$, at a majority of the
39 locations (Shackleton, 1987; 2000; Lambeck et al., 2014). The ice volume changes induced well-defined shifts in
40 biogenic carbonate $\delta^{18}\text{O}$ during the last several million years. Therefore, the regional evaporation-precipitation, runoff
41 and temperature changes are reconstructed from the global ice-volume corrected biogenic carbonate $\delta^{18}\text{O}$ (Wang et
42 al., 1995; Kallel et al., 1997; Schmidt et al., 2004; Saraswat et al., 2012; 2013; Kessarkar et al., 2013).

43 The $\delta^{18}\text{O}$ of surface dwelling planktic foraminifera *Globigerinoides ruber* ($\delta^{18}\text{O}_{\text{ruber}}$) is often used to
44 reconstruct past surface seawater conditions (Saraswat et al., 2012; 2013; Mahesh and Banakar, 2014). Therefore,
45 continuous efforts are made to understand the factors affecting $\delta^{18}\text{O}_{\text{ruber}}$ (Vergnaud-Grazzini, 1976; Mulitza et al.,
46 1997; 2003; Waelbroeck et al., 2005; Mohtadi et al., 2011; Horikawa et al., 2015; Hollstein et al., 2017; ; Sanchez et
47 al., 2022). The depth habitat of *G. ruber* in the tropical Atlantic Ocean has been inferred from its stable oxygen isotopic
48 ratio (Farmer et al., 2007). The change in stable oxygen isotopic ratio of planktic foraminifera, including *G. ruber*, is
49 suggested as a proxy to reconstruct upper water column stratification in the tropical Atlantic Ocean, based on the good
50 correlation between $\delta^{18}\text{O}$ and the ambient seawater characteristics (Steph et al., 2009). A few studies suggested a
51 difference in the $\delta^{18}\text{O}$ of various morphotypes of *G. ruber* (sensu stricto and sensu lato) and attributed it to their distinct
52 ecology and depth habitat (Löwemark et al., 2005). However, a recent study from the Gulf of Mexico suggested a
53 similar ecology and depth habitat for both the *G. ruber* morphotypes (Thirumalai et al., 2014). The northern Indian
54 Ocean being influenced by huge fresh water influx as well as being a part of the Indo-Pacific Warm Pool (De Deckker,
55 2016), provides a unique setting to understand the effect of large salinity and temperature changes on $\delta^{18}\text{O}_{\text{ruber}}$. Earlier,
56 Duplessy et al., (1981) measured $\delta^{18}\text{O}$ of the living *G. ruber* specimens collected from the water column as well as of
57 the dead ones recovered from surface sediments of the northern Indian Ocean. A similar study from the Red Sea and
58 adjoining western Arabian Sea suggested that *G. ruber* calcifies its test in isotopic equilibrium with the ambient
59 seawater, thus tracking the inter-annual subtle change in the salinity and temperature (Kroon and Ganssen, 1989;
60 Ganssen and Kroon, 1991).

61 The temperature influence on $\delta^{18}\text{O}_{\text{ruber}}$ is well defined (Mulitza et al., 2003). The effect of fresh water influx
62 induced changes in ambient salinity on $\delta^{18}\text{O}_{\text{ruber}}$ is, however, debated (Dämmer et al., 2020). With the extensive use
63 of $\delta^{18}\text{O}_{\text{ruber}}$ to reconstruct regional evaporation-precipitation changes, especially from the monsoon dominated tropical
64 oceans, it is imperative to understand the precise influence of ambient salinity on $\delta^{18}\text{O}_{\text{ruber}}$. The ambient seawater pH,
65 carbonate ion concentration (Bijma et al., 1999), presence/absence of symbionts (Jørgensen et al., 1985) also affect
66 the isotopic composition of *G. ruber*. However, limited glacial-interglacial variability in these parameters is masked

67 by the dominance of temperature and fresh water influx induced salinity changes in oxygen isotopic ratio of *G. ruber*.
68 Additionally, the diagenetic changes, especially dissolution, also substantially alters the original isotopic composition
69 of the foraminifera shells (Berger and Killingley, 1977; Wu and Berger, 1989; Lohmann, 1995; McCorkle et al., 1997;
70 Wycech et al., 2018). The dissolution preferentially removes lighter oxygen isotopic ratio rich sections of the shells,
71 thus increasing the whole shell $\delta^{18}\text{O}_{ruber}$ (Berger and Gardner, 1975; Lohmann, 1995; Weinkauff et al., 2020). To The
72 studies based on the comparison of ambient parameters with the isotopic composition of living specimens collected
73 in plankton tows may not address the complete range of the changes in isotopic signatures during the sinking of the
74 tests from the surface waters post death, and its subsequent deposition in the sediments at the bottom of the sea. As
75 the fossil shells are the sole basis to find out the isotopic ratio of the ambient seawater in the past, the effect of
76 diagenetic changes including the dissolution on foraminifer's oxygen isotopic ratio has to be properly evaluated. Here,
77 we assess the influence of strong salinity gradient, depth induced dissolution and other associated parameters on the
78 stable oxygen isotopic ratio of the surface dwelling planktic foraminifera *G. ruber* (white variety) in the surface
79 sediments of the northern Indian Ocean.

80

81 **2. Ecology of *Globigerinoides ruber* (white)**

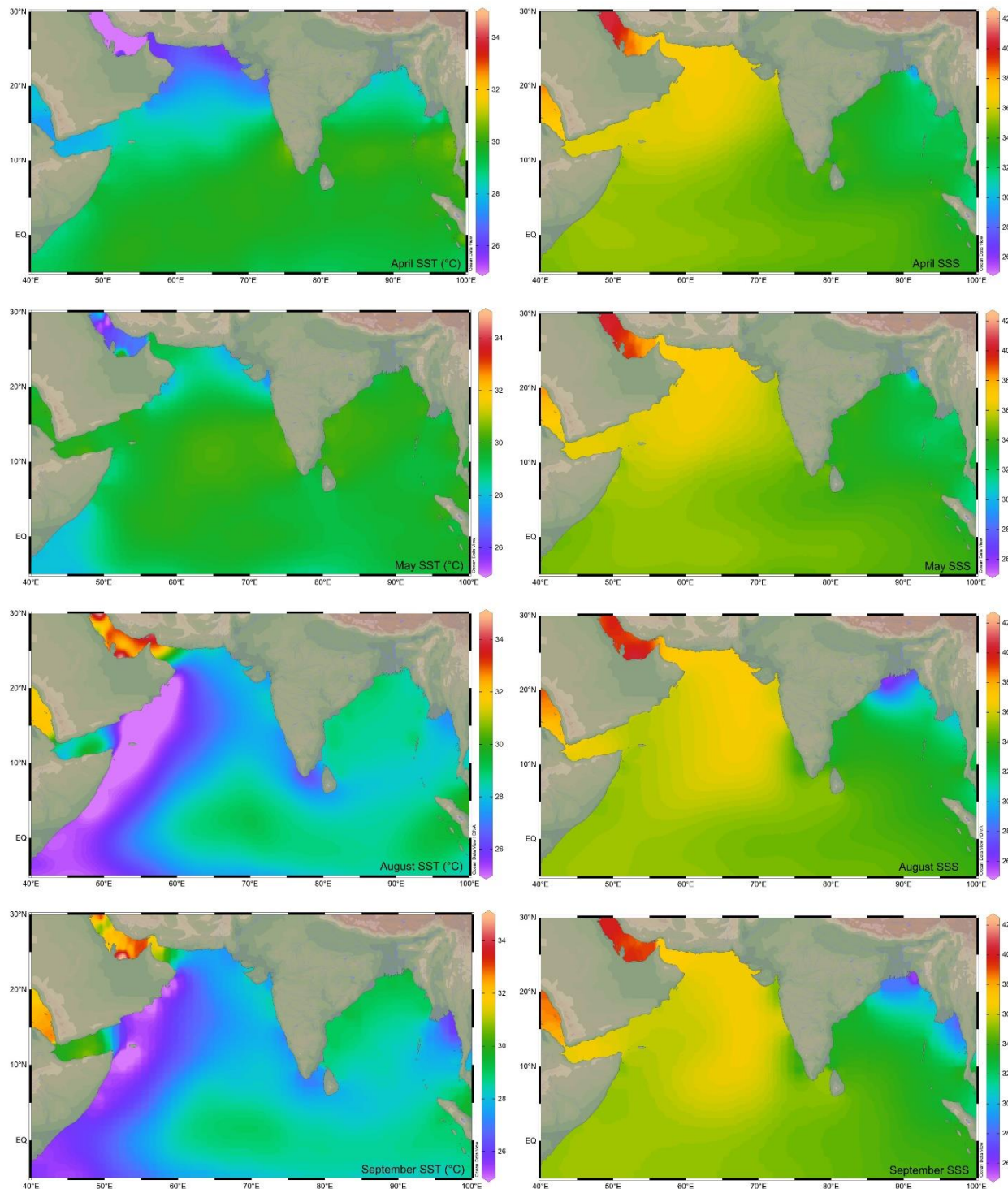
82 *Globigerinoides ruber* is a spinose planktic foraminifera inhabiting the mixed layer waters, throughout the year, in the
83 tropical-subtropical regions (Guptha et al. 1997; Kemle-von-Mücke and Hemleben 1999). It is one of the dominant
84 planktic foraminifera in the northern Indian Ocean (Bé and Hutson, 1977; Bhadra and Saraswat, 2021) with its relative
85 abundance being as high as ~60% (Fraile et al., 2008). Its test is medium to low trochospiral and hosts algal symbionts
86 (Hemleben et al., 1989). *Globigerinoides ruber* prefers to feed upon phytoplankton (Hemleben et al., 1989), and is
87 dominant in oligotrophic warmer water with optimal temperature being 23.5°C (Fraile et al., 2008). However, it is
88 amongst a few planktic foraminifera species that can tolerate a wide range of salinity (22-49 psu) and temperature
89 (14-31°C) (Hemleben et al., 1989; Guptha et al., 1997). Two varieties of *G. ruber*, namely the white and pink are
90 common in the world oceans. However, the pink variety of *G. ruber* became extinct in the Indian and Pacific Oceans
91 at ~120 kyr during the Marine Isotopic Stage 5e (Thompson et al., 1979).

92

93 **3. Northern Indian Ocean**

94 The Indian Ocean with its northern boundary in the tropics includes two hydrographically contrasting basins, namely
95 the Arabian Sea and Bay of Bengal (BoB) (Figure 1). The excess of evaporation over precipitation generates high
96 salinity water mass that spreads throughout the surface of the northern Arabian Sea with its core as deep as ~100 m
97 (Shetye et al., 1994; Prasanna Kumar and Prasad, 1999; Joseph and Freeland, 2005). Other high salinity water masses
98 from both the Persian Gulf and Red Sea enter the northern Arabian Sea at deeper depths between 200-400 m and 500-
99 800 m, respectively (Rochford, 1964). A strong upwelling along the western boundary of the Arabian Sea during the

100 summer monsoon season brings cold, nutrient rich subsurface waters to the surface (Chatterjee et al., 2019). The weak
101 upwelling during the same season is also reported in the southeastern Arabian Sea (Smitha et al., 2014).



102 **Figure 1: The sea surface temperature (SST) (°C) (Locarnini et al., 2018) and salinity (SSS) (psu) (Zweng et al., 2018) in the**
103 **northern Indian Ocean during the monsoon (August-September) and non-monsoon (April-May) months. The major rivers**
104

105 **draining into the northern Indian Ocean, are marked by blue lines. The map has been prepared by using Ocean Data View**
106 **software (Schlitzer, 2018).**

107
108 The surface water is relatively fresher in the BoB, as the majority of the rivers from the Indian sub-continent drain
109 here, with the total annual continental runoff accounting to 2950 km³ (Sengupta et al., 2006). Additionally, the total
110 annual precipitation over the BoB is 4700 km³, and the evaporation is 3600 km³ (Sengupta et al., 2006). The high
111 salinity Arabian Sea water is transported into the BoB and the fresher BoB water mixes with the high salinity Arabian
112 Sea water, by the seasonally reversing coastal currents (Shankar et al., 2002). The upwelling during summer is
113 restricted to only the northwestern part of the BoB (Shetye et al., 1991). The upwelling combined with the convective
114 mixing during the winter season in the north-eastern Arabian Sea (Madhupratap et al., 1996) as well as eddies in the
115 BoB (Prasanna Kumar et al., 2004; Sarma et al., 2020) result in very high primary productivity in both basins (Qasim,
116 1977; Prasanna Kumar et al., 2009). The high primary productivity and fresh water capping induce strong stratification
117 and restricted circulation that create oxygen deficient zones (ODZ) at the intermediate depth in both the Arabian Sea
118 (Rixen et al., 2020; Naqvi, 2021) and BoB (Bristow et al., 2016, Sridevi and Sarma, 2020). The Arabian Sea ODZ,
119 however, is comparatively thicker and intense, leading to denitrification (Naqvi et al., 2006), which is not reported yet
120 from the BoB (Bristow et al., 2016).

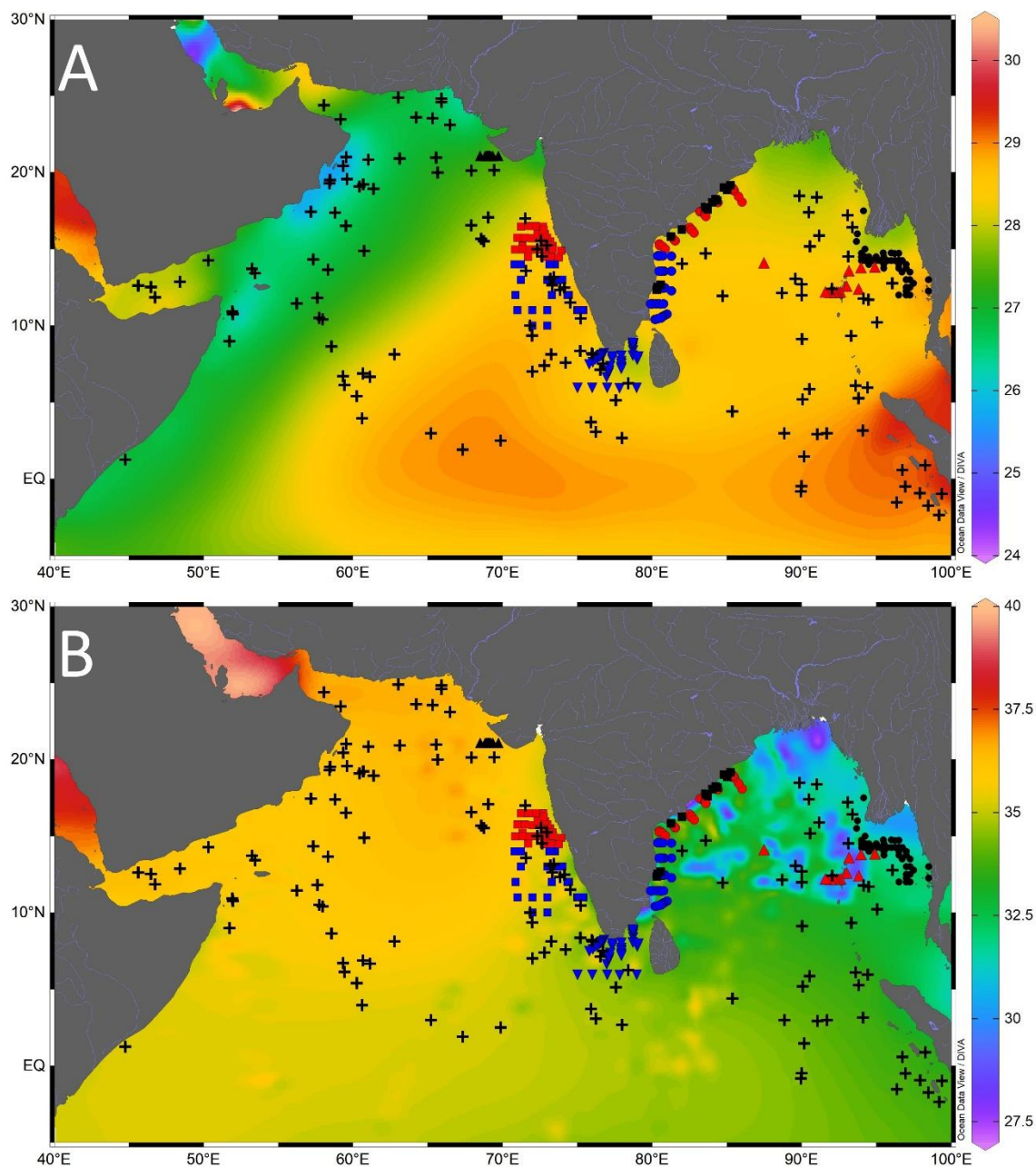
121 The equatorial Indian Ocean forms a part of the Indo-Pacific Warm Pool with sea surface temperature >28
122 °C throughout the year (Vinayachandran and Shetye, 1991; De Deckker, 2016). The marginal regions of the BoB are
123 comparatively warmer due to the fresh water influx from the rivers. The riverine influx shoals the mixed layer and
124 thickens the barrier layer, a buoyant layer separating the thermocline from the pycnocline, in the BoB (Howden and
125 Murtugudde, 2001). The riverine influx flows as a low salinity tongue all along the eastern margin of India (Chaitanya
126 et al., 2014). The annual average sea surface salinity (SSS) is <34 psu throughout the BoB, increasing from the head
127 bay towards south. In contrast to that, SSS remains >35 psu almost throughout the year in the Arabian Sea (Rao and
128 Sivakumar, 2003). The excess of evaporation over precipitation due to the dry northeasterly winds leads to the highest
129 salinity in the northern BoB during the winter (Rao and Sivakumar, 2003).

130

131 **4. Materials and Methodology**

132 The surface sediments were collected all along the path of seasonal coastal currents in the northern Indian Ocean
133 (Figure 2, Supplementary Table 1). The samples from the Ayeyarwady Delta Shelf in the northeastern BoB were
134 collected during 'India–Myanmar Joint Oceanographic Studies' onboard Ocean Research Vessel *Sagar Kanya*
135 (SK175). A total of 110 surface sediment samples were collected from the water depths ranging from 10 m to 1080
136 m, on the Ayeyarwady Delta Shelf (Ramaswamy et al., 2008). The multicore samples were also collected at regular
137 intervals in transects running perpendicular to the coast, from the western BoB during the cruise SK308, onboard
138 Research Vessel *Sindhu Sadhana* (cruise SSD067) and Research Vessel *Sindhu Sankalp* (cruise SSK35). A total of
139 84 surface samples (including 71 multicore samples and 13 grab samples from sandy sediments) were collected from

140 the inner shelf to outer slope region of the eastern margin of India during the cruise SK308 (Suokhrie et al., 2021a;
141 Saalim et al., 2022). These samples from the western BoB represent the lowest salinity region in the northern Indian
142 Ocean (Panchang and Nigam, 2012). The multicore samples collected between 25 m and 2980 m in the Gulf of Mannar
143 and the region west of it (43 samples onboard Research Vessel *Sindhu Sadhana* SSD004) represent the zone of cross-
144 basin exchange of seawater between the BoB and the Arabian Sea (Singh et al., 2021). The spade core samples
145 collected from the southeastern Arabian Sea (ORV *Sagar Kanya* cruise SK117 and SK237) are located close to the
146 distal end of the low salinity BoB water intruding into the Arabian Sea. The multicore samples (13 number) collected
147 during SSD055 cruise, from the northeastern Arabian Sea, represent the warm saline conditions. We also collected
148 spade core surface samples from the Andaman Sea, onboard Research Vessel *Sindhu Sankalp* (cruise SSK98). A total
149 of 252 samples had sufficient *G. ruber* for isotopic analysis (Table 1). The new data was augmented with 148
150 previously published core-top studies (e.g. Sirocko, 1989; Prell and Curry, 1981; Duplessy et al., 1981; 1982).
151 Therefore, a total of 400 surface sample data points were used for this study.



152
 153
 154
 155
 156
 157
 158
 159
 160

Figure 2: Location of the core top samples analyzed in this study (black filled triangle - cruise SSD055, red filled square - cruise SK117, blue filled square - cruise SK237, blue filled inverted triangle - cruise SSD004, blue filled circle - cruise SSD067, red filled circle - cruise SK308, black filled square - cruise SSK035, red filled triangle - cruise SSK098, black filled circle - cruise SK175) and the previously published core top values (black plus) compiled from the northern Indian Ocean. The background contours are temperature ($^{\circ}\text{C}$) (A) and salinity (psu) (B) with the scale on the right. Major rivers draining into the northern Indian Ocean, are marked by blue lines. The map has been prepared by using Ocean Data View software (Schlitzer, 2018).

161

162 **Table 1: Details of the expedition, number of samples collected in each expedition and the region in which the expedition**
 163 **was held to collect the surface sediment samples used in this study.**

Sr.No.	Cruise	Month/Year	Area	Total Samples
1.	SK117	September-October 1996	Eastern Arabian Sea	27
2.	SK175	April-May 2002	North-eastern Bay of Bengal	45
3.	SK237	August 2007	South-eastern Arabian Sea	26
4.	SK308	January 2014	Northwestern Bay of Bengal	29
5.	SSD004	October-November 2014	Gulf of Mannar, Lakshadweep Sea	41
6.	SSD055	August 2018	North-eastern Arabian Sea	11
7.	SSD067	November-December 2019	South-western Bay of Bengal, Lakshadweep Sea, Eastern Arabian Sea	45
8.	SSK035	May-June 2012	Western Bay of Bengal	13
9.	SSK098	January-February 2017	Andaman Sea	15

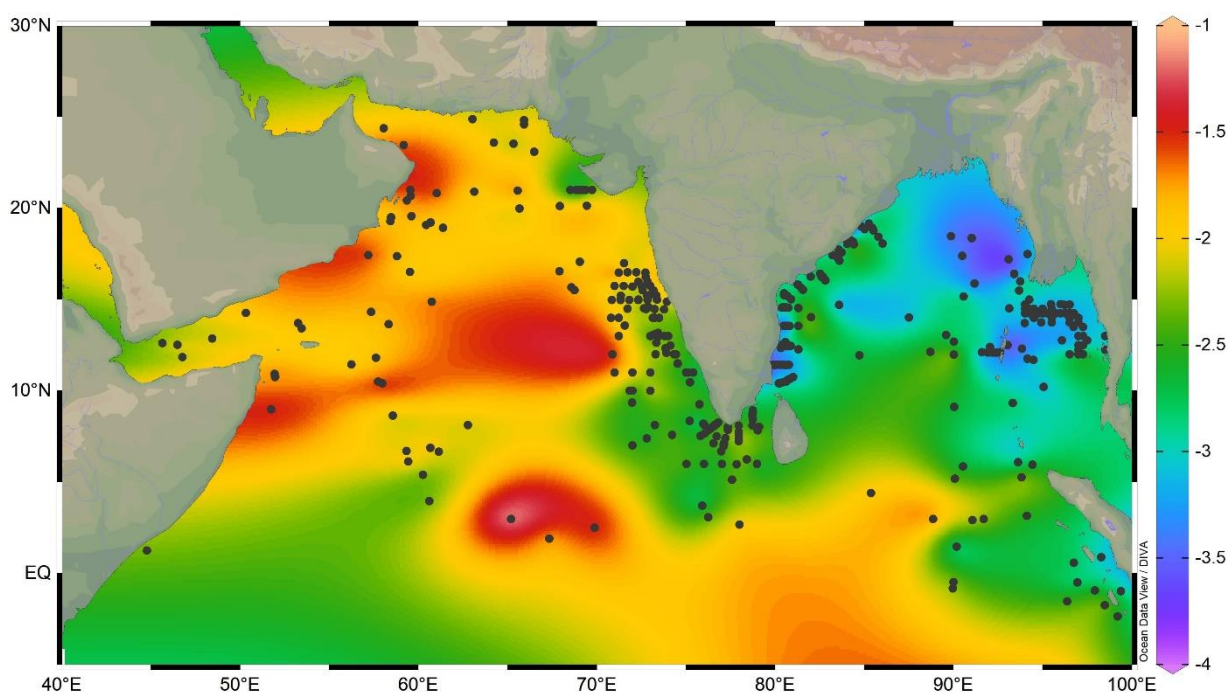
164
 165 The surface sediment samples (0-1 cm) were processed following the standard procedure (Suokhrie et al., 2021b). The
 166 freeze-dried sediments were weighed and wet sieved by using 63 μm sieve. The coarse fraction ($>63 \mu\text{m}$) was dry
 167 sieved by using 250 μm and 355 μm sieves. For $\delta^{18}\text{O}$ analysis, 10-15 well preserved shells of *G. ruber* white variety
 168 were picked from 250-355 μm size range. We picked *G. ruber* s.s. wherever sufficient specimens were available.
 169 Unfortunately, several samples yielded very small carbonate fraction. In such samples, we picked mixed population
 170 of *G. ruber* to get sufficient specimens for isotopic analysis. The $\delta^{18}\text{O}_{ruber}$ was measured by using Finnigan MAT 253
 171 isotope ratio mass spectrometer, coupled with Kiel IV automated carbonate preparation device. The samples were
 172 analyzed in the Alfred Wegner Institute for Polar and Marine Research, Bremerhaven, MARUM, University of
 173 Bremen, Bremen, Germany and the Stable Isotope Laboratory (SIL) at Indian Institute of Technology, Roorkee, India.
 174 The reference material NBS 18 limestone was used as the calibration material and a secondary in-house standard was
 175 run after every 5 samples to detect and correct the drift. The precision of oxygen isotope measurements was better
 176 than 0.08‰. The $\delta^{18}\text{O}_{ruber}$ data generated on the newly collected surface sediments was augmented with the published
 177 core-top $\delta^{18}\text{O}$ measurements in the northern Indian Ocean. A total of 400 surface sediment data points (252 from this
 178 work and 148 from the previous studies) were used to understand the factors affecting $\delta^{18}\text{O}_{ruber}$ in the northern Indian
 179 Ocean (Supplementary Table 1). The annual average sea surface temperature and salinity of the top 30 m water column
 180 at the respective sample locations was downloaded from the World Ocean Atlas (Boyer et al., 2013). The salinity and
 181 temperature at the core location was extrapolated from the nearby grid points, using the Live Access Server at the
 182 National Institute of Oceanography, Goa, India.

183 The analyzed $\delta^{18}\text{O}_{ruber}$ data was compared with the expected $\delta^{18}\text{O}$ calcite to ascertain whether the *G. ruber*
 184 properly represents the ambient conditions. For the expected $\delta^{18}\text{O}$ calcite, the $\delta^{18}\text{O}_{sw}$ was calculated from the ambient
 185 salinity by using the regional seawater salinity and its stable oxygen isotopic ($\delta^{18}\text{O}_{sw}$) ratio for the entire northern

186 Indian Ocean (5°S to 30°N). The seawater salinity and corresponding $\delta^{18}\text{O}_{\text{sw}}$ data was downloaded from the Schmidt
187 et al., (1999) (version 1.22) and augmented with other regional datasets (Delaygue et al., 2001; Singh et al., 2010;
188 Achyuthan et al., 2013).
189

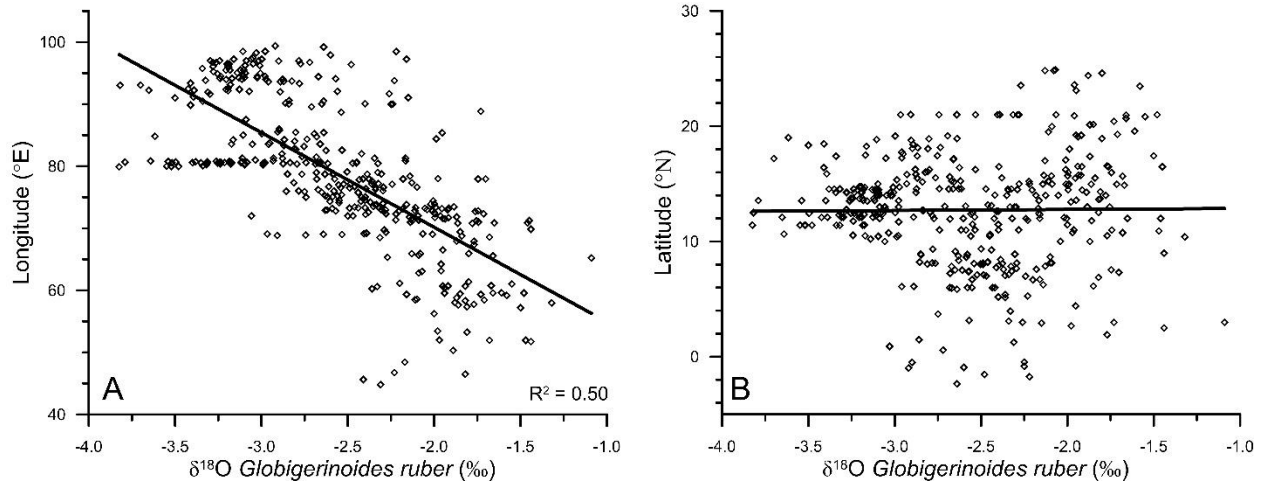
190 5. Results

191 The oxygen isotopic ratio of *G. ruber* varies from a minimum of -3.82‰ to the maximum of -1.09‰ in the surface
192 sediments of the northern Indian Ocean (Figure 3). The most depleted $\delta^{18}\text{O}_{\text{ruber}}$ was in the eastern BoB and the most
193 enriched values were in the western Arabian Sea.



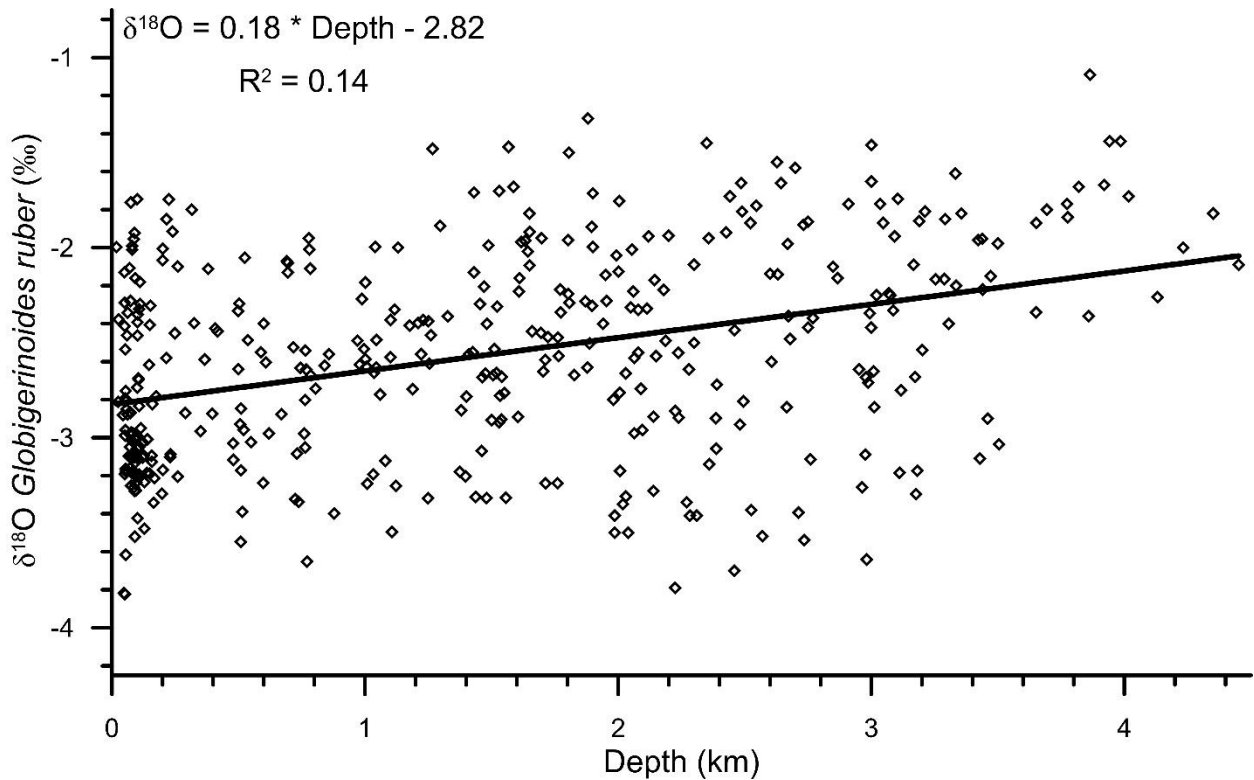
194
195 **Figure 3:** The variation in *Globigerinoides ruber* $\delta^{18}\text{O}$ (‰) in the surface sediments of the northern Indian Ocean. The
196 stations are marked by black filled circle. The lowest $\delta^{18}\text{O}_{\text{ruber}}$ is in the riverine influx influenced northern Bay of Bengal
197 and the highest is in the evaporation dominated central and western Arabian Sea. The major rivers are marked with thin
198 blue lines. The map has been prepared by using Ocean Data View software (Schlitzer, 2018).
199

200
201 The east-west gradient in $\delta^{18}\text{O}_{\text{ruber}}$ was also evident in its significant correlation ($R^2 = 0.5$, $n = 400$) with the longitude
202 (Figure 4A). However, $\delta^{18}\text{O}_{\text{ruber}}$ did not have any systematic latitudinal variation (Figure 4B).



203
 204 **Figure 4:** The variation in *Globigerinoides ruber* $\delta^{18}\text{O}$ (‰) with the corresponding longitude (A) and latitude (B), in the
 205 surface sediments of the northern Indian Ocean.
 206

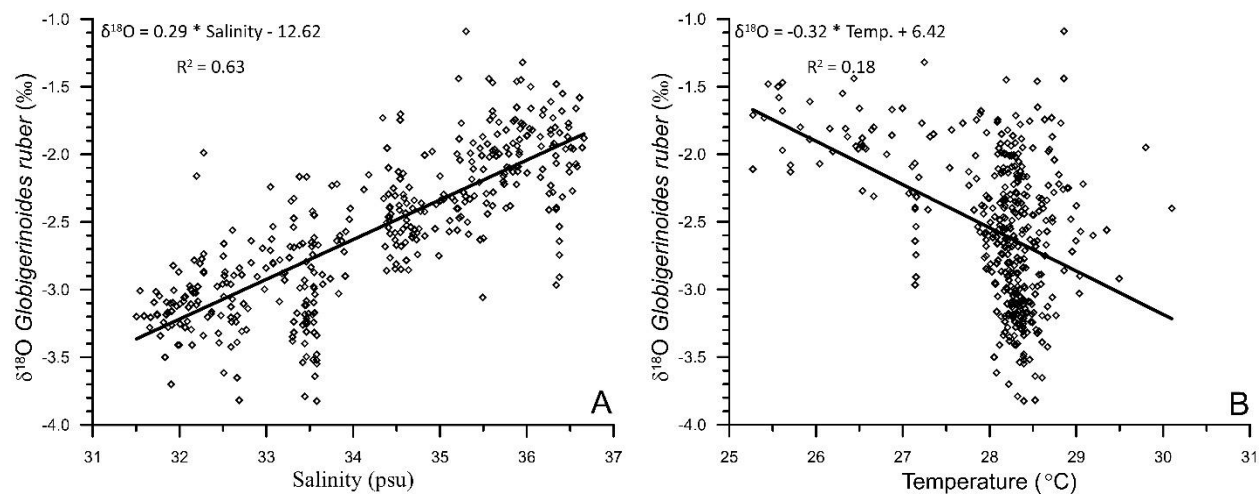
207
 208 A significant correlation ($R^2 = 0.14$, $n = 400$) was observed between the water depth and $\delta^{18}\text{O}_{\text{ruber}}$ (Figure 5). $\delta^{18}\text{O}_{\text{ruber}}$
 209 increased with increasing depth. The increase was gradual, without any abrupt change.



210
 211
 212 **Figure 5:** The relationship between water depth and the oxygen isotopic ratio of mixed layer dwelling *Globigerinoides ruber*.
 213 The trendline signifies the relative enrichment of $\delta^{18}\text{O}_{\text{ruber}}$ shells in surface sediments, with increasing water depth.
 214

215
216
217
218
219
220

The uncorrected $\delta^{18}\text{O}_{ruber}$ was significantly correlated ($R^2 = 0.63$, $n = 400$) with the ambient salinity (Figure 6A). However, the relationship between uncorrected $\delta^{18}\text{O}_{ruber}$ and ambient temperature was not as robust ($R^2 = 0.18$, $n = 400$) (Figure 6B). A large scatter ($\sim -3.8\%$ to -1.4%) was observed in the $\delta^{18}\text{O}_{ruber}$ of the samples collected from a narrow range of ambient temperature (28-29°C) (Figure 6B).

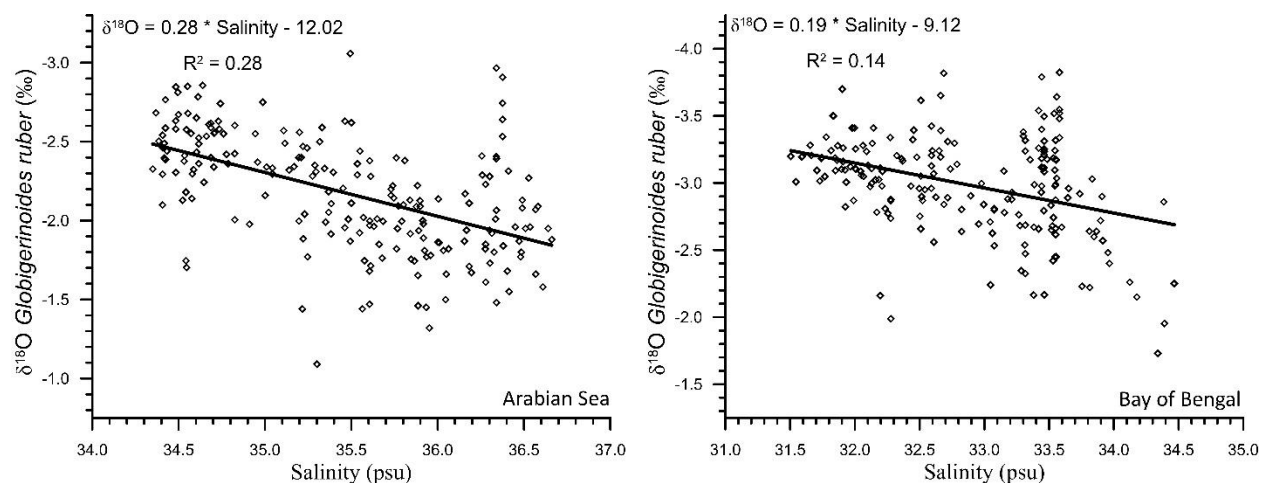


221
222
223
224
225

Figure 6: The relationship between stable oxygen isotopic ratio of mixed layer dwelling *Globigerinoides ruber* and annual average mixed layer salinity (A) and temperature (B) in the northern Indian Ocean.

226
227
228
229
230

As the northern Indian Ocean includes two contrasting basins, $\delta^{18}\text{O}_{ruber}$ -salinity relationship was explored for both the Arabian Sea and the BoB. A significant $\delta^{18}\text{O}_{ruber}$ -salinity relationship was observed for both the Arabian Sea ($R^2 = 0.28$, $n = 205$) and BoB ($R^2 = 0.14$, $n = 195$) (Figure 7). We report a different $\delta^{18}\text{O}_{ruber}$ -salinity relationship in these two basins. $\delta^{18}\text{O}_{ruber}$ increased with increasing salinity in both the BoB and the Arabian Sea.



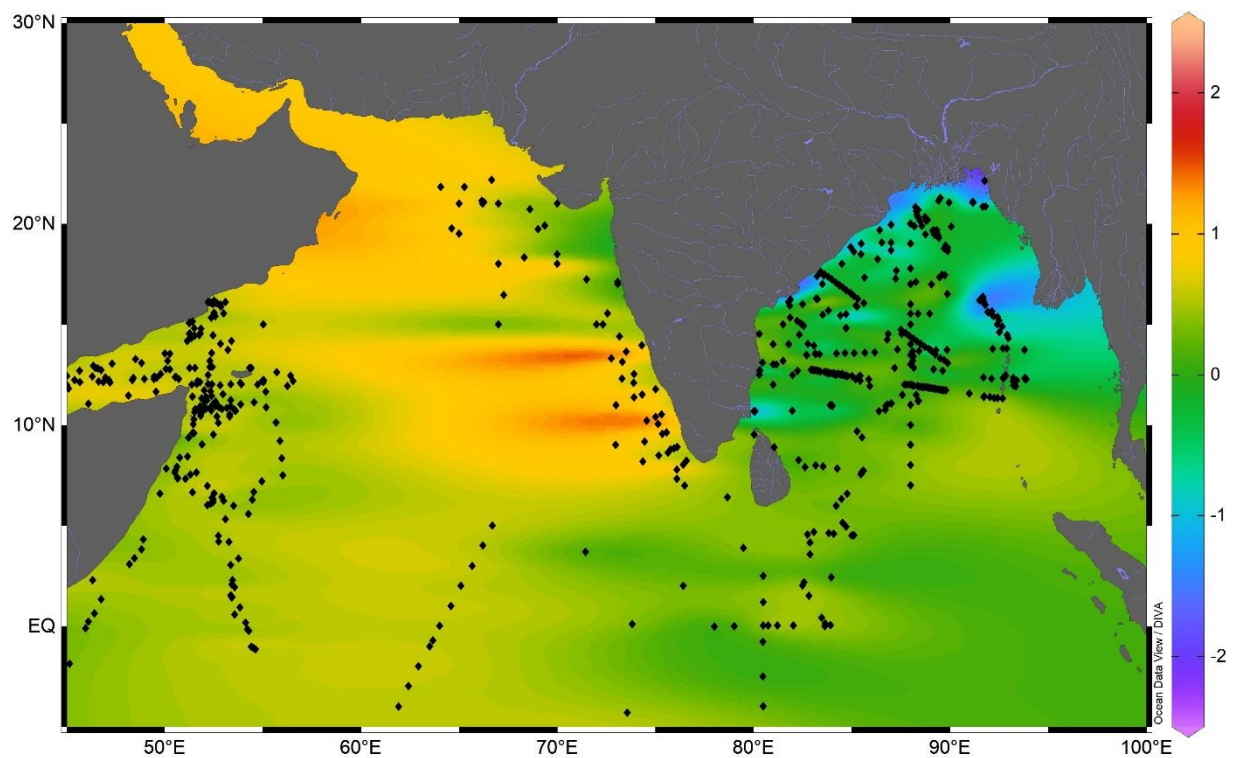
231

232
233
234
235

Figure 7: The relationship between the stable oxygen isotopic ratio of mixed layer dwelling *Globigerinoides ruber* and annual average mixed layer salinity in the Arabian Sea and Bay of Bengal.

236

237 The dataset to derive the regional salinity- $\delta^{18}\text{O}_{\text{sw}}$ relationship comprises of a total of 750 stations with salinity varying
238 from 20.92 psu to 40.91 psu. The dataset also covered a large range of $\delta^{18}\text{O}_{\text{sw}}$, varying from a minimum of -2.45‰ to
239 the maximum of 2.02‰ (Figure 8, 9). The measured $\delta^{18}\text{O}_{\text{ruber}}$ is strongly correlated ($R^2 = 0.56$, $n = 400$) with the
240 expected $\delta^{18}\text{O}_{\text{calcite}}$, as estimated by using the salinity- $\delta^{18}\text{O}_{\text{sw}}$ relationship and the ambient temperature. However, the
241 relationship between seawater temperature and $\delta^{18}\text{O}_{\text{ruber}}-\delta^{18}\text{O}_{\text{sw}}$, was not very robust. It should however, be noted here
242 that the stratigraphic information is not provided for most of the core tops. Core top sediments can represent older
243 time slices when the sedimentation rates are low or when older sediments are exposed due to erosional processes. This
244 does not matter so much if the Holocene is present and stable. However, in the Indian Ocean, large Holocene $\delta^{18}\text{O}$
245 variations are expected due to variations in monsoon precipitation. Therefore, the uncertain age of the core tops can
246 affect the results stated above.



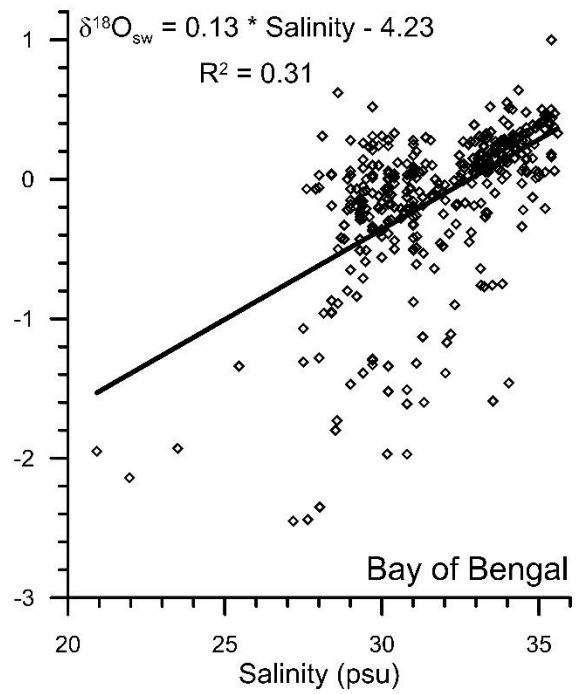
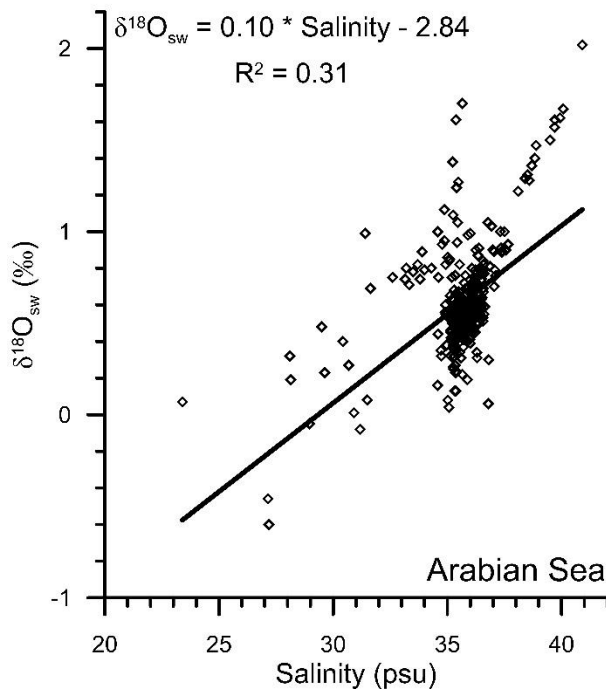
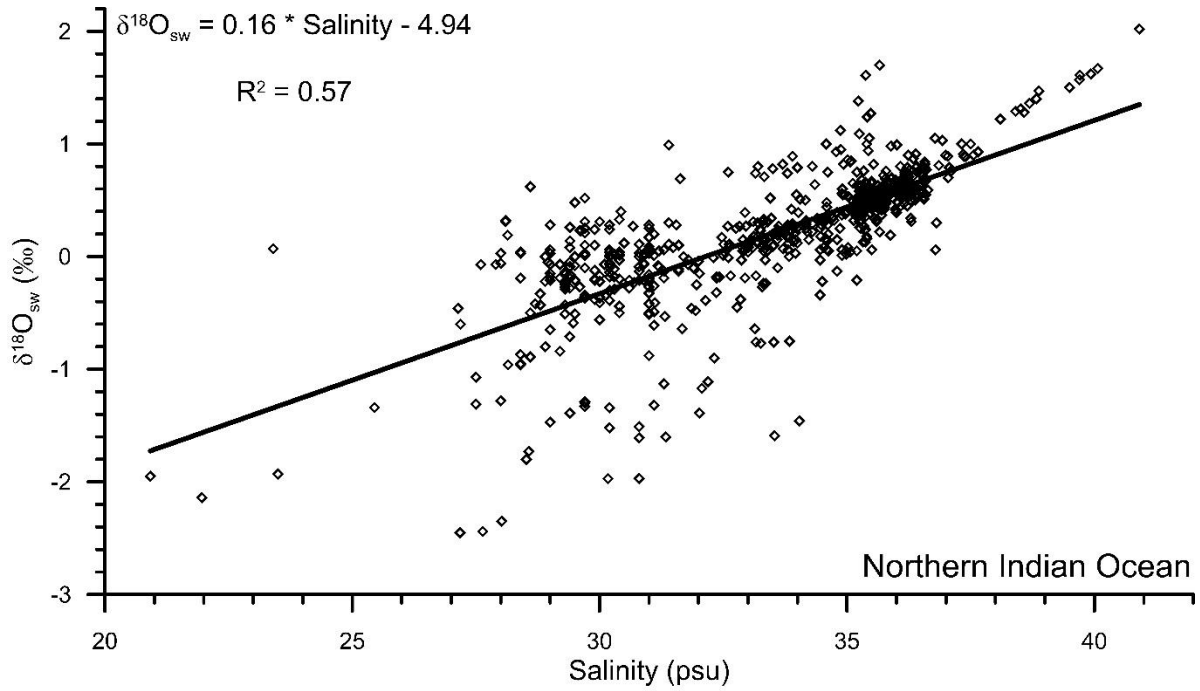
247

248

249

Figure 8: The surface seawater oxygen isotopic ratio (‰) in the northern Indian Ocean. The black filled circles are the seawater sample locations compiled from previous studies. The thin blue lines are the major rivers draining in the northern Indian Ocean. The map has been prepared by using Ocean Data View software (Schlitzer, 2018).

252



253
 254
 255

256 **Figure 9:** The relationship between surface water oxygen isotopic ratio and salinity in the northern Indian Ocean (5°S-
 257 30°N), Arabian Sea and the Bay of Bengal. The data points are from Schmidt et al., (1999), Delaygue et al., (2001), Singh et
 258 al., (2010), and Achyuthan et al., (2013).

259

260 6. Discussion

261 6.1 Expected versus analyzed $\delta^{18}\text{O}$

262 The estimation of expected $\delta^{18}\text{O}$ carbonate requires known seawater $\delta^{18}\text{O}$ values. The seawater $\delta^{18}\text{O}$, however, was
263 not measured. Therefore, the salinity- $\delta^{18}\text{O}_{\text{sw}}$ relationship established from the previous regional seawater isotope and
264 salinity measurements was used. The salinity- $\delta^{18}\text{O}_{\text{sw}}$ relationship varies seasonally as well as from region to region
265 (Singh et al., 2010; Achyuthan et al., 2013; Tiwari et al., 2013). Therefore, it was difficult to choose the appropriate
266 salinity- $\delta^{18}\text{O}_{\text{sw}}$ relationship. Initially, all the data points were clubbed to establish the salinity- $\delta^{18}\text{O}_{\text{sw}}$ relationship. By
267 comparing the measured $\delta^{18}\text{O}_{\text{sw}}$ with the ambient salinity, we established the following relationship for the entire
268 northern Indian Ocean (north of 5°S latitude) ($R^2 = 0.57$, $n = 750$) (Figure 9).

269

$$270 \delta^{18}\text{O}_{\text{sw}} = 0.16 * \text{Salinity} - 4.94 \quad \text{Northern Indian Ocean } (R^2 = 0.57)$$

271

272 Previously, a large difference in the slope of salinity- $\delta^{18}\text{O}_{\text{sw}}$ equation has been reported from the Arabian Sea and the
273 BoB (Delaygue et al., 2001; Singh et al., 2010; Achyuthan et al., 2013). Therefore, we also plotted the salinity- $\delta^{18}\text{O}_{\text{sw}}$
274 separately for the Arabian Sea and BoB (Figure 9). The salinity- $\delta^{18}\text{O}_{\text{sw}}$ relationship for these two basins was
275 represented by the following equations.

276

$$277 \delta^{18}\text{O}_{\text{sw}} = 0.10 * \text{Salinity} - 2.84 \quad \text{Arabian Sea} \quad (R^2 = 0.31, n = 375)$$

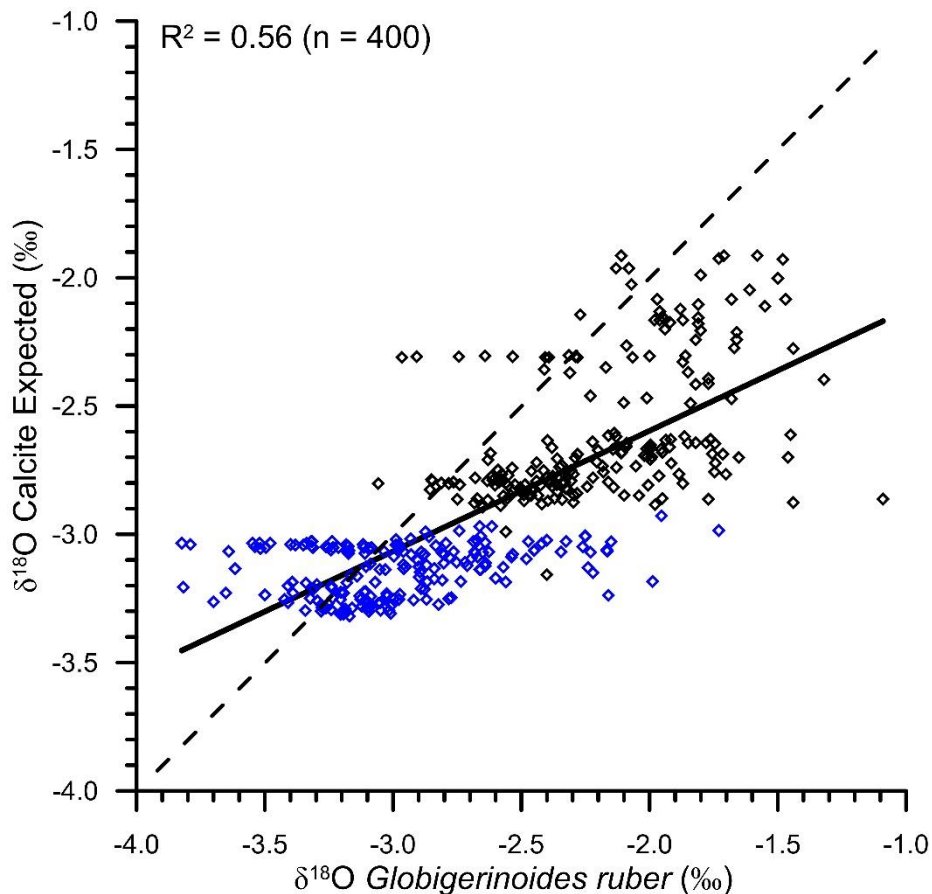
278

$$279 \delta^{18}\text{O}_{\text{sw}} = 0.13 * \text{Salinity} - 4.23 \quad \text{Bay of Bengal} \quad (R^2 = 0.31, n = 375)$$

280

281 The continuous flux of *G. ruber* throughout the year (Guptha et al., 1997) and the accumulation of shells in the
282 sediments over a large interval, implies that the salinity- $\delta^{18}\text{O}_{\text{sw}}$ relationship based on data representing all seasons will
283 provide a better estimate of the average $\delta^{18}\text{O}_{\text{ruber}}$ as recovered from the sediments (Vergnaud-Grazzini, 1976). The
284 expected $\delta^{18}\text{O}_{\text{sw}}$ was calculated by using these equations and the annual average mixed layer salinity at the stations
285 for which $\delta^{18}\text{O}_{\text{ruber}}$ data were available. The mixed layer was defined as the top 25 m of the water column following
286 Narvekar and Prasanna Kumar (2014). Although the mixed layer depth varies regionally as well as during different
287 seasons, the average mixed layer depth was used to compare the calcification conditions. A correction factor of 0.27‰
288 was applied to convert $\delta^{18}\text{O}_{\text{sw}}$ from SMOW to PDB scale (Hut, 1987). The expected $\delta^{18}\text{O}$ calcite was then estimated
289 from the calculated $\delta^{18}\text{O}_{\text{sw}}$ and the annual average mixed layer temperature by using the equation proposed by Mulitza
290 et al., (2003). We also estimated the expected $\delta^{18}\text{O}$ calcite by using the high-light equation of Bemis et al (1998), as
291 *G. ruber* $\delta^{18}\text{O}$ is better described with the high-light equation (Thunell et al. 1999). The choice of equation used to
292 estimate the expected $\delta^{18}\text{O}$ calcite did not make any difference other than a small offset. The difference between
293 expected $\delta^{18}\text{O}$ calcite estimated using paleotemperature equation of Mulitza et al., (2003) and the high-light equation
294 of Bemis et al., (1998) varied from -0.33 to -0.41‰. The expected $\delta^{18}\text{O}$ calcite estimated using Mulitza et al., (2003)
295 paleotemperature equation provided values close to the measured *G. ruber* $\delta^{18}\text{O}$. From the scatter plot (Figure 10), it

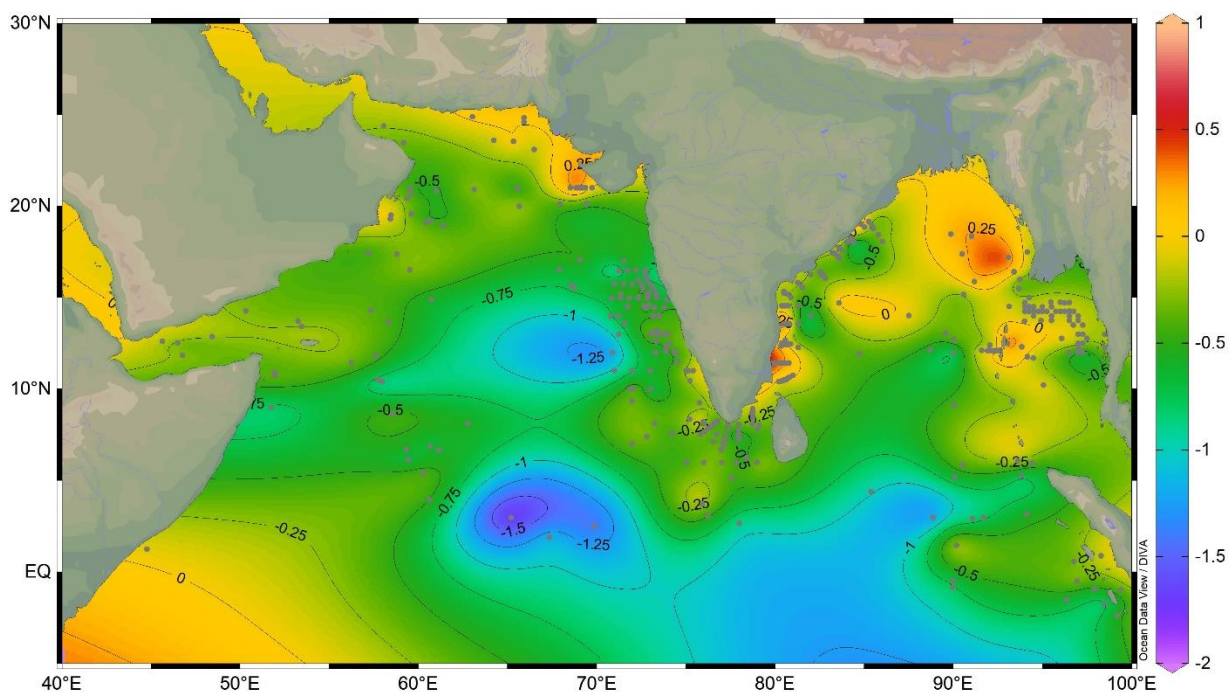
296 was clear that the analyzed $\delta^{18}\text{O}_{ruber}$ was significantly correlated ($R^2 = 0.56$, $n = 400$) with the expected $\delta^{18}\text{O}$ calcite,
 297 suggesting that *G. ruber* correctly represents the ambient conditions in the entire northern Indian Ocean. The expected
 298 $\delta^{18}\text{O}$ calcite estimated by using the separate Arabian Sea and BoB salinity- $\delta^{18}\text{O}_{sw}$ equations, was also similarly
 299 correlated with the analyzed $\delta^{18}\text{O}_{ruber}$.



300
 301
 302 **Figure 10:** The scatter plot of expected $\delta^{18}\text{O}$ calcite (as estimated from the ambient salinity-temperature) and the analyzed
 303 $\delta^{18}\text{O}_{ruber}$. The two are significantly correlated ($R^2 = 0.56$), suggesting that *Globigerinoides ruber* correctly represents the
 304 ambient conditions. The blue diamonds are the samples collected from the Bay of Bengal and the black diamonds represent
 305 the samples collected from the Arabian Sea. The dotted line represents the 1:1 relationship between the measured and
 306 expected $\delta^{18}\text{O}$.

307
 308 The deviation of the expected $\delta^{18}\text{O}_{calcite}$ from the observed $\delta^{18}\text{O}_{ruber}$ ($\delta^{18}\text{O}_{residual}$) can be because of several factors
 309 including the difference in the ambient conditions at the time of secretion of the primary calcite during the lifetime
 310 and the diagenetic changes post death and burial. The observed $\delta^{18}\text{O}_{ruber}$ was close to the expected $\delta^{18}\text{O}_{calcite}$ in the
 311 shallower waters, especially the BoB, Andaman Sea and northeastern Arabian Sea (Figure 11). The difference was
 312 large in the deeper Arabian Sea and the equatorial Indian Ocean. *Globigerinoides ruber* is suggested to inhabit
 313 chlorophyll maximum for easy availability of food (Fairbanks and Weibe, 1980). In such a scenario, $\delta^{18}\text{O}_{ruber}$ is
 314 expected to be higher due to lower temperatures and lower light levels at relatively deeper depths (Spero et al., 1997).
 315 The depth of chlorophyll maximum is shallower in the marginal marine waters of both the BoB and the Arabian Sea

316 (Sarma & Aswanikumar, 1991; Madhu et al., 2006). If *G. ruber* thrived at chlorophyll maximum depths, the $\delta^{18}\text{O}_{ruber}$
 317 should be enriched in heavier isotope and thus $\delta^{18}\text{O}_{residual}$ should be negative. The positive $\delta^{18}\text{O}_{residual}$ in the shallower
 318 regions, however, suggests that *G. ruber* thrives in the warmer upper parts of the mixed layer. Alternatively, the large
 319 influence of the depleted fresh water $\delta^{18}\text{O}$ dominates the chlorophyll maximum influence on the observed $\delta^{18}\text{O}_{ruber}$ in
 320 the shallower regions of the northern Indian Ocean. The concentration of positive $\delta^{18}\text{O}_{residual}$ values close to the riverine
 321 influx regions confirms the strong influence of depleted fresh water $\delta^{18}\text{O}$ in modulating $\delta^{18}\text{O}_{ruber}$ in the northern Indian
 322 Ocean. The negative $\delta^{18}\text{O}_{residual}$ at deeper stations is attributed to a combination of factors including deeper chlorophyll
 323 maximum depth habitat of *G. ruber*, reduced influence of fresh water, lower sedimentation rate resulting in mixing of
 324 older and younger fauna, and post depositional diagenetic changes.



325
 326 **Figure 11: The difference in the expected $\delta^{18}\text{O}_{calcite}$ and observed $\delta^{18}\text{O}_{ruber}$ in the surface sediments of the northern Indian**
 327 **Ocean. The grey filled squares are the sample locations. The thin blue lines are the major rivers draining in the northern**
 328 **Indian Ocean. The thin black lines mark the contours at 0.25‰ interval. The map has been prepared by using Ocean Data**
 329 **View software (Schlitzer, 2018).**

330

331 **6.2 Latitudinal and Longitudinal variation in $\delta^{18}\text{O}_{ruber}$**

332 We report a strong ($R^2 = 0.50$) longitudinal influence on $\delta^{18}\text{O}_{ruber}$. A similar relationship with the latitudes is missing.
 333 The strong longitudinal signature in $\delta^{18}\text{O}_{ruber}$ is attributed to the large salinity gradient. The huge fresh water influx in
 334 the BoB reduces the SSS in the eastern Indian Ocean. The lack of major rivers in the western Arabian Sea results in
 335 strong low to high salinity gradient from east to west. Although the equatorial and nearby regions are a part of the

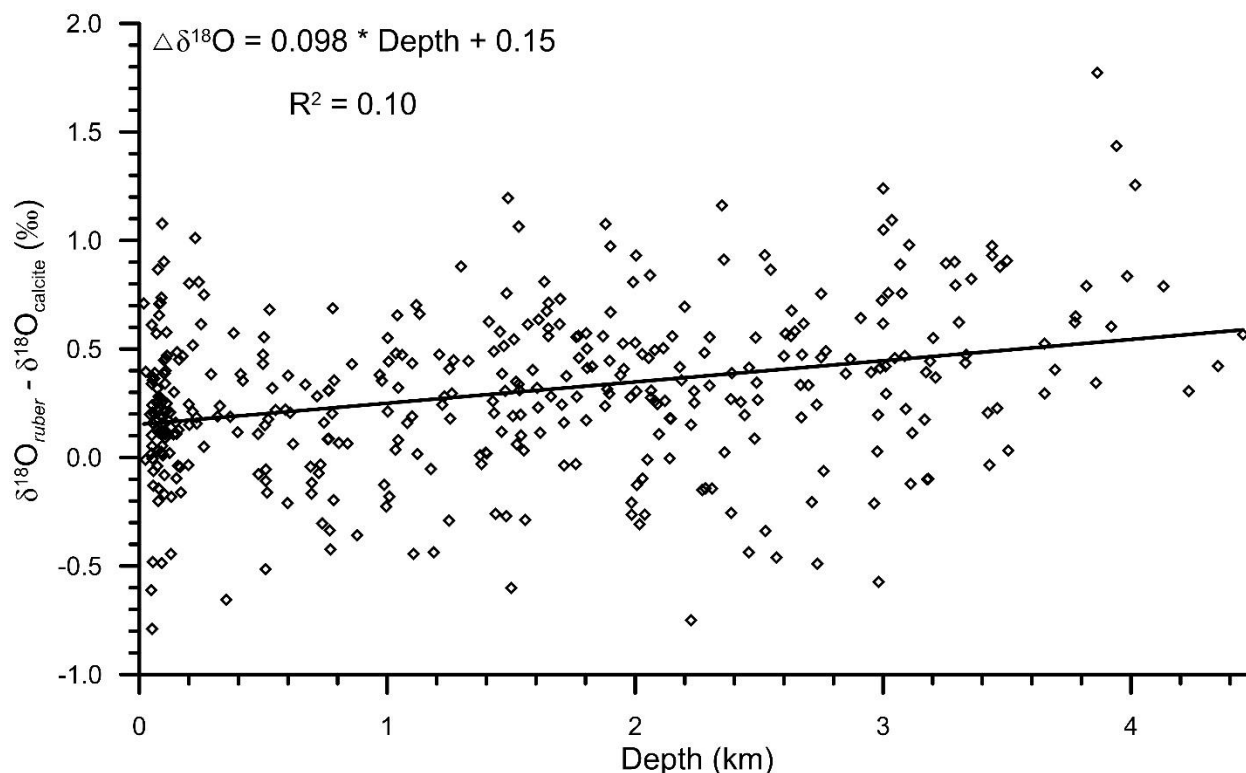
336 Indo-Pacific Warm Pool, the limited temperature variability is evident in the insignificant latitudinal influence on
337 $\delta^{18}\text{O}_{ruber}$.
338

339 **6.3 Diagenetic alteration**

340 We found a strong diagenetic overprinting of $\delta^{18}\text{O}_{ruber}$ in the northern Indian Ocean (Figure 5). The enrichment of
341 $\delta^{18}\text{O}_{ruber}$ with increasing water depth suggests either dissolution leading to the preferential removal of chambers with
342 higher fraction of the lighter oxygen isotope (Wycech et al., 2018), or secondary calcification under comparatively
343 colder water (Lohmann, 1995; Schrag et al., 1995). The increase in planktic foraminifera $\delta^{18}\text{O}$ with increasing depth
344 is a common diagenetic alteration throughout the world oceans (Bonneau et al., 1980). Interestingly, the extent of the
345 increase in $\delta^{18}\text{O}_{ruber}$ with depth in the northern Indian Ocean is much smaller (0.18‰ per thousand meters) than that
346 reported for the same species from the Pacific Ocean (0.4‰ per thousand meters) (Bonneau et al., 1980). However,
347 the increase in $\delta^{18}\text{O}_{ruber}$ with depth in the northern Indian Ocean is continuous, unlike the abrupt shift in $\delta^{18}\text{O}$ (0.3-
348 0.4‰, between the depths above and below the lysocline) of another surface dwelling planktic species, namely
349 *Trilobatus sacculifer*, as observed in the western equatorial Pacific (Wu and Berger, 1989). The smaller increase in
350 $\delta^{18}\text{O}_{ruber}$ with depth is attributed to the shallower habitat of *G. ruber* as compared to *T. sacculifer*. The chamber
351 formation at different water depths implies increased heterogeneity in the *T. sacculifer* shells, with those formed at
352 warmer surface temperature being more susceptible to dissolution as compared to those formed at deeper depths during
353 the gametogenesis phase (Wycech et al., 2018). The chambers in *G. ruber* are formed at a similar depth and therefore,
354 the increase in $\delta^{18}\text{O}_{ruber}$ is continuous, while those of *T. sacculifer* are precipitated at different depths and therefore the
355 shift in $\delta^{18}\text{O}$ after a particular depth. The increase in $\delta^{18}\text{O}_{ruber}$ with depth is mainly due to the partial dissolution of the
356 more porous and thinner parts of the shells secreted at warmer temperature, as such parts are comparatively more
357 susceptible to dissolution (Berger, 1971). The increase in $\delta^{18}\text{O}_{ruber}$ with depth is similar in both the Arabian Sea and
358 BoB.

359 Additionally, the gradual decrease in the sedimentation rate with increasing depth and distance from the
360 continental margins can also cause a depth related trend in $\delta^{18}\text{O}_{ruber}$. The bioturbation disturbs the top few cm
361 sediments (Gerino et al., 1998) resulting in the mixing of older shells with comparatively younger shells (Löwemark,
362 and Grootes, 2004). In high sedimentation rate regions of the shelf and slope, the mixing is restricted to the shells
363 deposited in a shorter, climatologically stable interval. However, in the deeper regions, it is likely that the shells
364 deposited during the colder glacial interval or deglaciation with relatively higher $\delta^{18}\text{O}_{ruber}$ gets mixed with the younger
365 shells, as it is available close to the surface due to the low sedimentation rate (Broecker, 1986; Anderson, 2001). The
366 mixing of shells with a relatively higher $\delta^{18}\text{O}$ with the modern shells having lighter $\delta^{18}\text{O}$ can also result in the depth
367 related increasing trend of $\delta^{18}\text{O}_{ruber}$. The sedimentation rate is very high on the slope and decreases in the deeper
368 regions of both the Arabian Sea (Singh et al., 2017) and BoB (e.g. Bhonsale and Saraswat, 2012; Suokhrie et al.,
369 2022).

370 The large influence of the terrestrial fresh water influx in the shallower region, as compared to the deeper
 371 parts of the northern Indian Ocean, is also likely to contribute to the observed increase in $\delta^{18}\text{O}_{ruber}$ with depth. The
 372 fresh water is depleted in heavier oxygen isotope as compared to the seawater (Bhattacharya et al., 1985; Ramesh &
 373 Sarin, 1992). Thus, the foraminiferal shells secreted in the shallow waters are likely to be enriched in the lighter
 374 oxygen isotope, resulting in a depth related bias. Therefore, to delineate the influence of depth related diagenetic
 375 alteration and secondary calcification in $\delta^{18}\text{O}_{ruber}$, we subtracted the expected $\delta^{18}\text{O}_{calcite}$ from the measured $\delta^{18}\text{O}_{ruber}$.
 376 The difference between the measured $\delta^{18}\text{O}_{ruber}$ and expected $\delta^{18}\text{O}_{calcite}$ was plotted with water depth (Figure 12). The
 377 difference (measured $\delta^{18}\text{O}_{ruber}$ - expected $\delta^{18}\text{O}_{calcite}$) increased with depth, suggesting a strong influence of the depth
 378 related processes in $\delta^{18}\text{O}_{ruber}$.



379
 380 **Figure 12: The relationship of the difference between measured $\delta^{18}\text{O}_{ruber}$ and expected $\delta^{18}\text{O}_{calcite}$ with the water depth from**
 381 **which the surface samples were collected, in the northern Indian Ocean. The $\delta^{18}\text{O}_{ruber} - \delta^{18}\text{O}_{calcite}$ increased with increasing**
 382 **water depth.**

383

384 6.4 Salinity contribution to $\delta^{18}\text{O}_{ruber}$

385 We report a strong influence of salinity on $\delta^{18}\text{O}_{ruber}$ ($R^2=0.63$). As expected, $\delta^{18}\text{O}_{ruber}$ has a direct positive relationship
 386 with the ambient salinity. The $\delta^{18}\text{O}_{ruber}$ increased by 0.29‰ for every psu increase in salinity. The northern Indian
 387 Ocean has a large salinity gradient (~10 psu) from the lowest in the northern BoB to the highest in the northwestern
 388 Arabian Sea. The river water and direct precipitation is enriched in the lighter isotope (Kumar et al., 2010; Kathayat
 389 et al., 2021). Thus, the increased riverine influx and precipitation contributes isotopically lighter water to the surface

390 ocean (Rai et al., 2021) and decreases the $\delta^{18}\text{O}_{ruber}$. From the surface seawater samples collected during the winter
391 monsoon season (January-February 1994), a $\delta^{18}\text{O}$ -salinity slope of 0.26‰ was deduced for the Arabian Sea and of
392 0.18‰ for the BoB (Delaygue et al., 2001). However, the $\delta^{18}\text{O}$ -salinity slope varies regionally as well as during
393 different seasons (Singh et al., 2010; Achyuthan et al., 2013). The $\delta^{18}\text{O}$ -salinity slope varied from as low as 0.10 for
394 the coastal BoB samples collected during the months of April-May to as high as 0.51 for the samples collected from
395 the western BoB during the peak south-west monsoon season (August-September 1988) (Singh et al., 2010). The large
396 seasonal variation implies limitations of $\delta^{18}\text{O}$ -salinity slope deduced from snapshot surface seawater samples.
397 Additionally, *G. ruber* flux is reported throughout the year (Guptha et al., 1997), suggesting that the fossil population
398 represents annual average conditions (Thirumalai et al., 2014).

399 A different $\delta^{18}\text{O}_{ruber}$ -salinity slope for the Arabian Sea (0.28) and BoB (0.19) is attributed to the different
400 hydrographic regimes of these two basins. The runoff and precipitation excess in the BoB results in a comparatively
401 lower salinity as compared to the evaporation dominated Arabian Sea. However, it should be noted here that the
402 relationship between $\delta^{18}\text{O}_{ruber}$ and salinity was very robust for all the northern Indian Ocean samples plotted together.
403 Interestingly, the slope of $\delta^{18}\text{O}$ -salinity for the entire northern Indian Ocean samples is much lower than that for the
404 Atlantic Ocean (0.59 for North Atlantic and 0.52 for South Atlantic, Delaygue et al., 2000) despite the large meltwater
405 influx into the north Atlantic. The dissimilar $\delta^{18}\text{O}$ -salinity slope in different basins and also during different seasons
406 in the same basin is mainly attributed to the variation in the end member composition and the relative amount of fresh
407 water (riverine/precipitation/sub-marine ground water discharge) input from various sources during different seasons
408 (Achyuthan et al., 2013; Tiwari et al., 2013). The heavier oxygen isotope depleted precipitation/fresh water influx in
409 the higher latitudes (~35 ‰) as compared to the tropical areas (~5 ‰) also results in a higher slope of the $\delta^{18}\text{O}$ -
410 salinity relationship in the North Atlantic Ocean (Rozanski et al., 1993). Additionally, the difference in $\delta^{18}\text{O}$ -salinity
411 slope despite of the huge fresh water input into both the basins is also because a large fraction of the riverine fresh
412 water spreads across the surface of the northern Indian Ocean, while the melt water sinks to deeper depths in the North
413 Atlantic Ocean. A consistent systematic difference has previously been observed between planktic foraminiferal shells
414 collected in plankton tows and surface sediments, with shells from the sediments being comparatively enriched in ^{18}O
415 (Vergnaud-Grazzini, 1976).

416

417 **6.5 Temperature control on $\delta^{18}\text{O}_{ruber}$**

418 A first order comparison of the uncorrected $\delta^{18}\text{O}_{ruber}$ with ambient temperature of the top 30 m of the water column at
419 respective stations showed 0.32‰ decrease with every 1°C warming. The change in $\delta^{18}\text{O}_{ruber}$ as inferred from the
420 core-top sediments of the northern Indian Ocean is higher than that estimated from the plankton tows (0.22‰ per 1°C
421 change in temperature) (Mulitza et al., 2003). The seawater temperature was amongst the primary factors identified
422 to affect $\delta^{18}\text{O}_{ruber}$ (Emiliani, 1954; Mulitza et al., 2003). The low correlation between $\delta^{18}\text{O}_{ruber}$ and temperature in this
423 dataset is attributed to the limited temperature variability (1°C, 28-29°C) at a majority of the stations. The large salinity
424 difference (~6.5 psu) between stations further obscures any significant correlation between uncorrected $\delta^{18}\text{O}_{ruber}$ and

425 temperature. The temperature influence on $\delta^{18}\text{O}_{ruber}$ was thus assessed by comparing the ambient temperature with the
426 $\delta^{18}\text{O}_{ruber}$ corrected for $\delta^{18}\text{O}_{sw}$ ($\delta^{18}\text{O}_{ruber} - \delta^{18}\text{O}_{sw}$). The pH of the seawater has also been identified as a factor affecting
427 the stable oxygen isotopic composition of planktic foraminifera (Bijma et al., 1999). However, as argued by Mulitza
428 et al., (2003), the limited modern surface seawater pH variability (Chakraborty et al., 2021) and its close dependence
429 on temperature implies that the pH contribution to $\delta^{18}\text{O}_{ruber}$ is well within the error associated with the measurements.
430 The seawater pH in the immediate vicinity of the foraminiferal shell is strongly influenced by the light intensity in the
431 presence of symbionts (Jorgensen et al., 1985). The riverine influx in the northern Indian Ocean makes the surface
432 waters turbid reducing the light penetration depths (Prasanna Kumar et al., 2010). Therefore, riverine influx induced
433 variations in turbidity in the northern Indian Ocean can influence the $\delta^{18}\text{O}_{ruber}$ via the pH effect.

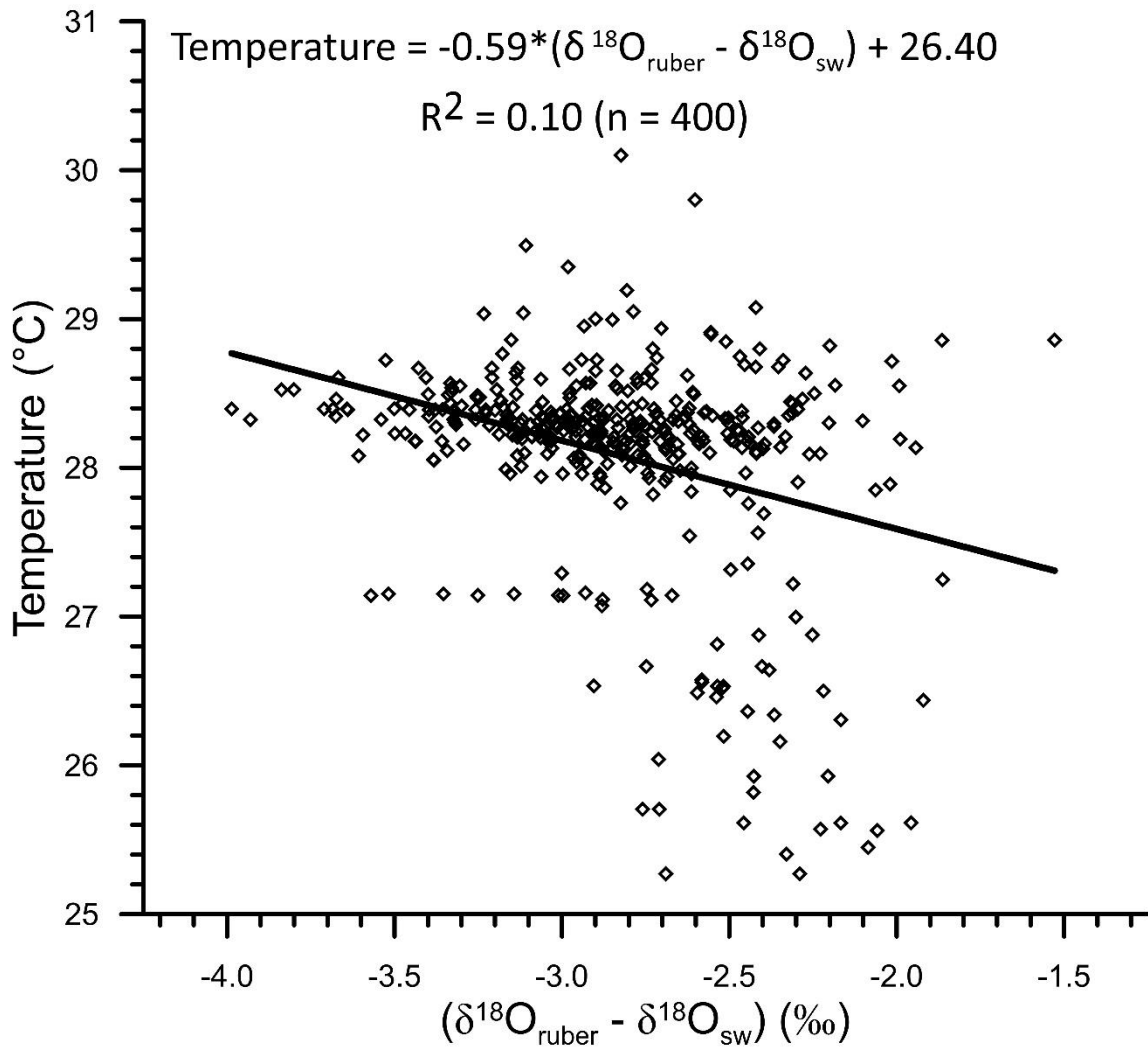
434 The comparison of $\delta^{18}\text{O}_{sw}$ corrected $\delta^{18}\text{O}_{ruber}$ with the ambient temperature also confirms the enrichment of
435 ($\delta^{18}\text{O}_{ruber} - \delta^{18}\text{O}_{sw}$) in heavier oxygen isotope with the decrease in temperature (Figure 13). We obtained the following
436 relationship between temperature and ($\delta^{18}\text{O}_{ruber} - \delta^{18}\text{O}_{sw}$) in the northern Indian Ocean.

437

$$438 \text{ Temperature} = -0.59 * (\delta^{18}\text{O}_{ruber} - \delta^{18}\text{O}_{sw}) + 26.40$$

439

440 The slope of the temperature and ($\delta^{18}\text{O}_{ruber} - \delta^{18}\text{O}_{sw}$) was somewhat different (0.17‰ per 1°C change in temperature)
441 than that of the temperature versus uncorrected $\delta^{18}\text{O}_{ruber}$, but similar as that reported for the plankton tows (0.22‰ per
442 1°C change in temperature) (Mulitza et al., 2003).



443
444

445 **Figure 13:** The relationship between ambient temperature and $(\delta^{18}\text{O}_{\text{ruber}} - \delta^{18}\text{O}_{\text{sw}})$ for the northern Indian Ocean. As
 446 expected the $(\delta^{18}\text{O}_{\text{ruber}} - \delta^{18}\text{O}_{\text{sw}})$ gets enriched in heavier isotope with decreasing ambient temperature.

447

448 **7. Conclusions**

449 We measured the stable oxygen isotopic ratio of the surface dwelling planktic foraminifera *Globigernoides ruber*
 450 white variety from the surface sediments of the northern Indian Ocean. A comparison of the $\delta^{18}\text{O}_{\text{ruber}}$ with the depth
 451 suggests a strong diagenetic alteration of the isotopic ratio. The ambient salinity exerts the maximum influence on the
 452 $\delta^{18}\text{O}_{\text{ruber}}$ suggesting its robust application to reconstruct past salinity in the northern Indian Ocean. The large east-west
 453 salinity gradient in the northern Indian Ocean results in a strong longitudinal variation in $\delta^{18}\text{O}_{\text{ruber}}$. The temperature
 454 influence on $\delta^{18}\text{O}_{\text{ruber}}$ is subdued as compared to the effect of large salinity variation in the northern Indian Ocean. We

455 report a relatively smaller change in $\delta^{18}\text{O}_{ruber}$ with a unit increase in ambient temperature in case of specimens retrieved
456 from the surface sediments as compared to those collected live from the water column.

457 **8. Data Availability**

458 The newly generated data as well as the data compiled from previous studies from the northern Indian Ocean has been
459 submitted to PANGAEA and is available at
460 <https://www.pangaea.de/tok/59190adf9e4facf7ebb9ad555c0bce58a9a72bd9> (Saraswat et al., 2022). The data is
461 submitted with the manuscript as well, for the reviewers' scrutiny.

462 **9. Author Contribution**

463 RS designed the research, compiled and interpreted the data and wrote the manuscript. TS, DKN, DPS, SMS, MS,
464 GS, SRB, SRK picked the specimens for isotopic analysis. MM, ASM supervised the analysis. All authors edited and
465 contributed to the final manuscript.

466 **10. Competing Interests**

467 The authors declare that they have no conflict of interest.

468 **Acknowledgements**

469 We thank the crew onboard expeditions during which the surface sediment samples were collected. The authors thank
470 the Director, CSIR-National Institute of Oceanography for the facilities and funding. The technical personnel at the
471 Alfred-Wegener Institute for Polar and Marine Research, and MARUM, Bremen University, Germany are
472 acknowledged for the help in stable isotopic analysis. We thank Dr. V. Ramaswamy, CSIR-NIO for providing the
473 surface sediment samples collected from the Myanmar continental shelf. The authors also thank Dr. B.N. Nath for
474 providing the spade core-top samples from the eastern margin of India. We thank Dr. Alberto Sanchez, Centro
475 Interdisciplinario de Ciencias Marinas, Instituto Politécnico Nacional, La Paz, B.C.S, Mexico, and the anonymous
476 reviewer, for their constructive comments and suggestions that helped to improve the manuscript.

477

478

479 **References**

- 480
- 481 Achyuthan, H., Deshpande, R.D., Rao, M.S., Kumar, B., Nallathambi, T., Shashi Kumar, K., Ramesh, R.,
482 Ramachandran, P., Maurya, A.S., and Gupta, S.K.: Stable isotopes and salinity in the surface waters of the Bay of
483 Bengal: Implications for water dynamics and palaeoclimate. *Mar. Chem.*, 149, 51-62, 2013.
- 484 [Anderson, D.M.: Attenuation of millennial-scale events by bioturbation in marine sediments. *Paleoceanography*, 16,](#)
485 [352–357, 2001.](#)
- 486 Bé, A.W.H., and Hutson, W.H.: Ecology of planktonic foraminifera and biogeographic patterns of life and fossil
487 assemblages in the Indian Ocean. *Micropaleontology*, 23, 369, 1977.
- 488 Bemis, B.E., Spero, H.J., Bijma, J., and Lea, D.W.: Reevaluation of the oxygen isotopic composition of planktonic
489 foraminifera: Experimental results and revised paleotemperature equations. *Paleoceanography* 13, 150-160, 1998.
- 490 Berger, W.H.: Sedimentation of planktonic foraminifera. *Mar. Geol.*, 11, 325-358, 1971.
- 491 Berger, W.H., and Killingley, J.S.: Glacial-Holocene transition in deep-sea carbonates: selective dissolution and the
492 stable isotope signal. *Science*, 197, 563-566, 1977.
- 493 Bhadra, S.R., and Saraswat, R.: Assessing the effect of riverine discharge on planktic foraminifera: A case study from
494 the marginal marine regions of the western Bay of Bengal. *Deep Sea Res. II: Topical Stud. Oceanogra.*, 183,
495 104927, 2021.
- 496 Bhattacharya, S.K., Gupta, S.K. and Krishnamurthy, R.V.: Oxygen and hydrogen isotopic ratios in ground waters and
497 river waters from India. *Proc. Indian Acad. Sci. (Earth Planet. Sci.)*, 94, 283-295, 1985.
- 498 [Bhonsale, S., and Saraswat, R.: Abundance and size variation of *Globorotalia menardii* in the northeastern Indian](#)
499 [Ocean during the late Quaternary. *J. Geol. Soc. India*, 80, 771-782, 2012.](#)
- 500 Bijma, J., Spero, H.J., and Lea, D.W.: Reassessing foraminiferal stable isotope geochemistry: Impact of the oceanic
501 carbonate system (experimental results). In: Fischer, G., Wefer, G. (Eds.), *Use of Proxies in Paleoclimatology:*
502 *Examples from the South Atlantic*. Springer, Berlin, pp. 489-512, 1999.
- 503 Bonneau, M.-C., Vergnaud-Grazzini, C., and Berger, W.H.: Stable isotope fractionation and differential dissolution
504 in Recent planktonic foraminifera from Pacific box-cores. *Oceanologica Acta*, 3, 377-382, 1980.
- 505 Boyer, T. P., Antonov, J. I., Baranova, O. K., Garcia, H. E., Johnson, D. R., Mishonov, A. V., et al.: *World Ocean*
506 *Database*, 2013.
- 507 Bristow, L.A., Callbeck, C.M., Larsen, M., Altabet, M.A., Dekaezemacker, J., Forth, M., Gauns, M., Glud, R.N.,
508 Kuypers, M.M.M., Lavik, G., Milucka, J., Naqvi, S.W. A., Pratihary, A., Revsbech, N. P., Thamdrup, B., Treusch,
509 A.H., and Canfield, D. E.: N₂ production rates limited by nitrite availability in the Bay of Bengal oxygen minimum
510 zone. *Nat. Geosci.*, 10, 24-29, 2017.
- 511 [Broecker, W.S.: Oxygen isotope constraints on surface ocean temperatures. *Quat. Res.*, 26, 121–134,](#)
512 [https://doi.org/10.1016/0033-5894\(86\)90087-6](https://doi.org/10.1016/0033-5894(86)90087-6), 1986.
- 513 Chaitanya, A.V.S., Lengaigne, M., Vialard, J., Gopalakrishna, V.V., Durand, F., Kranthikumar, C., Amritash, S.,
514 Suneel, V., Papa, F., and Ravichandran, M.: Salinity measurements collected by fishermen reveal a “river in the
515 sea” flowing along the eastern coast of India. *Bull. American Met. Soc.*, 95, 1897-1908, 2014.

516 Chakraborty, K., Valsala, V., Bhattacharya, T., and Ghosh, J.: Seasonal cycle of surface ocean pCO₂ and pH in the
517 northern Indian Ocean and their controlling factors. *Progr. Oceanogra.*, 198, 102683, 2021.

518 Chatterjee, A., Kumar, B.P., Prakash, S., and Singh, P.: Annihilation of the Somali upwelling system during summer
519 monsoon. *Sci. Rep.*, 9, 1-14, 2019.

520 Dämmer, L.K., de Nooijer, L., van Sebille, E., Haak, J.G., and Reichert, G.-J.: Evaluation of oxygen isotopes and
521 trace elements in planktonic foraminifera from the Mediterranean Sea as recorders of seawater oxygen isotopes
522 and salinity. *Clim. Past*, 16, 2401-2414, 2020.

523 De Deckker, P.: The Indo-Pacific Warm Pool: critical to world oceanography and world climate. *Geosci. Lett.*, 3, 20,
524 2016.

525 Delaygue, G., Bard, E., Rollion, C., Jouzel, J., Stievenard, M., and Duplessy, J.-C.: Oxygen isotope/salinity
526 relationship in the northern Indian Ocean. *J. Geophys. Res.*, 106, 4565-4574, 2001.

527 Delaygue, G., J. Jouzel, and Dutay, J.C.: Oxygen 18–salinity relationship simulated by an oceanic general circulation
528 model. *Earth Planet. Sci. Lett.*, 178, 113-123, 2000.

529 Duplessy, J.C., Bé, A.W.H., and Blanc, P.L.: Oxygen and carbon isotopic composition and biogeographic distribution
530 of planktonic foraminifera in the Indian Ocean. *Palaeogeogra., Palaeoclimatol., Palaeoecol.*, 33, 9-46, 1981.

531 Duplessy, J.C.: Glacial to interglacial contrasts in the northern Indian Ocean. *Nature*, 295, 494-498, 1982.

532 Duplessy, J.C., Blanc, P.L., and Bé, A.W.H.: Oxygen-18 enrichment of planktonic foraminifera due to gametogenic
533 calcification below the euphotic zone. *Science*, 213, 1247-1250, 1981.

534 Emiliani, C.: Depth habitat of some species of pelagic foraminifera as indicated by oxygen isotope ratio. *American J.*
535 *Sci.*, 252, 149-158, 1954.

536 Erez, J., and Luz, B.: Experimental paleotemperature equation for planktonic foraminifera. *Geochim. Cosmochim.*
537 *Acta*, 47, 1025-1031, 1983.

538 Fairbanks, R. G. and Wiebe, P. H.: Foraminifera and chlorophyll maximum: vertical distribution, seasonal succession,
539 and paleoceanographic significance, *Science (New York, N.Y.)*, 209, 1524–1526,
540 <https://doi.org/10.1126/science.209.4464.1524>, 1980.

541 Fraile, I., Schulz, M., Mulitza, S., and Kucera, M.: Predicting the global distribution of planktonic foraminifera using
542 a dynamic ecosystem model. *Biogeosciences*, 5, 891-911, 2008.

543 Ganssen, G., and Kroon, D.: Evidence for Red Sea surface water circulation from oxygen isotopes of modern surface
544 waters and planktonic foraminiferal tests. *Paleoceanography*, 6, 73-82, 1991.

545 Gerino, M., Aller, R.C., Lee, C., Cochran, J.K., Aller, J.Y., Green, M.A. and Hirschberg, D.: Comparison of different
546 tracers and methods used to quantify bioturbation during a spring bloom: 234-Thorium, luminophores and
547 chlorophyll a. *Estuarine Coast. Shelf Sci.*, 46, 531–547, 1998.

548 Guptha, M.V.S., Curry, W.B., Ittekkot, V., and Muralinath, A.S.: Seasonal variation in the flux of planktic
549 foraminifera: Sediment trap results from the Bay of Bengal, northern Indian Ocean. *J. Foraminiferal Res.*, 27, 5-
550 19, 1997.

551 Hemleben, C., Spindler, M., and Anderson, O. R.: *Modern Planktonic Foraminifera*, Springer-Verlag, New York,
552 1989.

553 Hollstein, M., Mohtadi, M., Rosenthal, Y., Moffa Sanchez, P., Oppo, D., Martínez Méndez, G., Steinke, S., and
554 Hebbeln, D.: Stable oxygen isotopes and Mg/Ca in planktic foraminifera from modern surface sediments of the
555 Western Pacific Warm Pool: Implications for thermocline reconstructions. *Paleoceanography*, 32, 1174-1194,
556 2017.

557 Horikawa, K., Kodaira, T., Zhang, J., and Murayama, M.: $\delta^{18}\text{O}_{\text{sw}}$ estimate for *Globigerinoides ruber* from core-top
558 sediments in the East China Sea. *Progr. Earth Planet. Sci.*, 2, 19, 2015.

559 Howden, S. D., and Murtugudde, R.: Effects of river inputs into the Bay of Bengal. *J. Geophys. Res.*, 106(C9), 19825-
560 19844, 2001.

561 Hut, G.: Consultants group meeting on stable isotope reference samples for geochemical and hydrological
562 investigations. Report to the Director General, International Atomic Energy Agency, Vienna, 42 pp, 1987.

563 Jørgensen, B. B., Erez, J., Revsbech, P., and Cohen, Y.: Symbiotic photosynthesis in a planktonic foraminiferan,
564 *Globigerinoides sacculifer* (Brady), studied with microelectrodes. *Limnol. Oceanogr.*, 30, 1253–1267, 1985.

565 Joseph, S., and Freeland, H.J.: Salinity variability in the Arabian Sea. *Geophys. Res. Lett.*, 32, L09607, 2005.

566 Kallel, N., Paterne, M., Duplessy, J., Vergnaudgrazzini, C., Pujol, C., Labeyrie, L., Arnold, M., Fontugne, M., and
567 Pierre, C.: Enhanced rainfall in the Mediterranean region during the last Sapropel Event. *Oceanologica Acta*, 20,
568 1997.

569 Kathayat, G., Sinha, A., Tanoue, M., K. Yoshimura, H. Li, Zhang, H., and Cheng, H.: Interannual oxygen isotope
570 variability in Indian summer monsoon precipitation reflects changes in moisture sources. *Comm. Earth Environ.*,
571 2, 96, 2021.

572 Kemle-von-Mücke, S., and Hemleben, C.: Planktic Foraminifera. In: Boltovskoy E (ed) South Atlantic zooplankton.
573 Backhuys Publishers, Leiden, pp 43-67, 1999.

574 Kessarkar, P.M., Purnachadra Rao, V., Naqvi, S.W.A., and Karapurkar, S.G.: Variation in the Indian summer monsoon
575 intensity during the Bølling-Ållerød and Holocene. *Paleoceanography*, 28, 413-425, 2013.

576 Kim, S.T., and O'Neil, J.R.: Equilibrium and nonequilibrium oxygen isotope effects in synthetic carbonates. *Geochim.*
577 *Cosmochim. Acta*, 61, 3461-3475, 1997.

578 Kroon, D., and Ganssen, G.: Northern Indian Ocean upwelling cells and the stable isotope composition of living
579 planktonic foraminifers. *Deep-Sea Res.*, 36, 1219-1236, 1989.

580 Kumar, B., S. P. Rai, U. Saravana Kumar, S. K. Verma, P. Garg, S. V. Vijaya Kumar, R. Jaiswal, B. K. Purendra, S.
581 R. Kumar, and N.G. Pande: Isotopic characteristics of Indian precipitation. *Water Resource Res.*, 46, W12548,
582 2010.

583 Lambeck, K., H. Rouby, A. Purcell, Y. Sun, and M. Sambridge: Sea level and global ice volumes from the Last Glacial
584 Maximum to the Holocene. *Proc. Nat. Acad. Sci.*, 111, 15296–15303, 2014.

585 Lea, D.W.: Elemental and isotopic proxies of past ocean temperatures. *Treatise Geochem.*, 8, 373-397, 2014.

586 Locarnini, R. A., Mishonov, A. V., Baranova, O. K., Boyer, T. P., Zweng, M. M., Garcia, H. E., Reagan, J. R., Seidov,
587 D., Weathers, K., Paver, C. R. and Smolyar, I.: *World Ocean Atlas 2018, Volume 1: Temperature*. A. Mishonov
588 Technical Ed.; NOAA Atlas NESDIS 81, 52pp, 2018.

589 Lohmann, G. P.: A model for variation in the chemistry of planktonic foraminifera due to secondary calcification and
590 selective dissolution. *Paleoceanography*, 10, 445-457, 1995.

591 Löwemark, L., and Grootes, P.M.: Large age differences between planktic foraminifers caused by abundance
592 variations and Zoophycos bioturbation. *Paleoceanography*, 19, PA2001, doi:10.1029/2003PA000949, 2004.

593 Löwemark, L., Hong, W.-L., Yui, T.-F., and Hung, G.-W.: A test of different factors influencing the isotopic signal
594 of planktonic foraminifera in surface sediments from the northern South China Sea. *Mar. Micropaleontol.* 55, 49-
595 62, 2005.

596 Madhu, N.V., Jyothibabu, R., Maheswaran, P.A., Gerson, V.J., Gopalakrishnan, T.C., and Nair, K.K.C.: Lack of
597 seasonality in phytoplankton standing stock (chlorophyll a) and production in the western Bay of Bengal. *Cont.*
598 *Shelf Res.*, 26, 1868-1883, 2006.

599 Madhupratap, M., S.P. Kumar, P.M.A. Bhattathiri, M.D. Kumar, S. Raghukumar, K.K.C. Nair, and N. Ramaiah:
600 Mechanism of the biological response to winter cooling in the northeastern Arabian Sea. *Nature*, 384, 549-552,
601 1996.

602 Mahesh, B.S., and Banakar, V.K.: Change in the intensity of low-salinity water inflow from the Bay of Bengal into
603 the Eastern Arabian Sea from the Last Glacial Maximum to the Holocene: Implications for monsoon variations.
604 *Palaeogeogra., Palaeoclimatol., Palaeoecol.*, 397, 31-37, 2014.

605 McCorkle, D. C., Martin, P. A., Lea, D. W., and Klinkhammer, G.P.: Evidence of a dissolution effect on benthic
606 foraminiferal shell chemistry: $\delta^{13}\text{C}$, Cd/Ca, Ba/Ca, and Sr/Ca results from the Ontong Java Plateau.
607 *Paleoceanography*, 10, 699-714, 1997.

608 Metcalfe, B., Feldmeijer, W., and Ganssen, G.M.: Oxygen isotope variability of planktonic foraminifera provide clues
609 to past upper ocean seasonal variability. *Paleoceanogra. Paleoclimatol.*, 34, 374–393, 2019.

610 Mohtadi, M., Oppo, D.W., Lückge, A., DePol-Holz, R., Steinke, S., Groeneveld, J., Hemme, N., and Hebbeln, D.:
611 Reconstructing the thermal structure of the upper ocean: Insights from planktic foraminifera shell chemistry and
612 alkenones in modern sediments of the tropical eastern Indian Ocean. *Paleoceanography*, 26, PA3219, 2011.

613 Mulitza, S., Boltovskoy, D., Donner, B., Meggers, H., Paul, A., and Wefer, G.: Temperature: $\delta^{18}\text{O}$ relationships of
614 planktonic foraminifera collected from surface waters. *Palaeogeogra., Palaeoclimatol., Palaeoecol.*, 202, 143-152,
615 2003.

616 Mulitza, S., Dürkoop, A., Hale, W., Wefer, G., and Niebler, H.S.: Planktonic foraminifera as recorders of past surface-
617 water stratification. *Geology*, 25, 335-338, 1997.

618 Mulitza, S., Wolff, T., Pätzold, J., Hale, W., and Wefer, G.: Temperature sensitivity of planktic foraminifera and its
619 influence on the oxygen isotope record. *Mar. Micropaleontol.*, 33, 223-240, 1998.

620 Naqvi, S.W.A.: Deoxygenation in marginal seas of the Indian Ocean. *Front. Mar. Sci.*, 8, 624322. doi:
621 10.3389/fmars.2021.624322, 2021.

622 Naqvi, S.W.A., H. Naik, A. Pratihary, W. D'souza, P.V. Narvekar, D.A. Jayakumar, A.H. Devol, T. Yoshinari, and T.
623 Saino: Coastal versus open-ocean denitrification in the Arabian Sea. *Biogeosciences*, 3, 621-633, 2006.

624 Panchang, R., and Nigam, R.: High resolution climatic records of the past~ 489 years from Central Asia as derived
625 from benthic foraminiferal species, *Asterorotalia trispinosa*. *Mar. Geol.*, 307, 88-104, 2012.

626 Pearson, P.N.: Oxygen isotopes in foraminifera: Overview and historical review. In *Reconstructing Earth's Deep-*
627 *Time Climate—The State of the Art in 2012*, Paleontological Society Short Course, November 3, 2012. The
628 Paleontological Society Papers, Volume 18, Linda C. Ivany and Brian T. Huber (eds.), pp. 1-38, 2012.

629 Prasanna Kumar, S., J. Narvekar, M. Nuncio, M. Gauns, and S. Sardesai: What drives the biological productivity of
630 the northern Indian Ocean? *Washington DC American Geophysical Union Geophysical Monograph Series*, 185,
631 33-56, 2009.

632 [Prasanna Kumar, S., Narvekar, J., Nuncio, M., Kumar, A., Ramaiah, N., Sardesai, S., Gauns, M., Fernandes, V., and
633 Paul J.: Is the biological productivity in the Bay of Bengal light limited? *Curr. Sci.*, 98, 1331-1339, 2010.](#)

634 Prasanna Kumar, S., M. Nuncio, J. Narvekar, A. Kumar, D.S. Sardesai, S.N. De Souza, M. Gauns, N. Ramaiah, and
635 M. Madhupratap: Are eddies nature's trigger to enhance biological productivity in the Bay of Bengal? *Geophys.*
636 *Res. Lett.*, 31, L07309, doi:10.1029/2003GL019274, 2004.

637 Prasanna Kumar, S., and Prasad, T.G.: Formation and spreading of Arabian Sea high-salinity water mass. *J. Geophys.*
638 *Res: Oceans*, 104, 1455-1464, 1999.

639 Prell, W.L., and Curry, W.B.: Faunal and isotopic indices of monsoonal upwelling: Western Arabian Sea.
640 *Oceanologica Acta*, 4, 91-98, 1981.

641 Qasim, S.Z.: Biological productivity of the Indian Ocean. *Indian J. Mar. Sci.*, 6, 122–137, 1977.

642 Rai, S.P., J. Noble, D. Singh, Y.S. Rawat, and B. Kumar: Spatiotemporal variability in stable isotopes of the Ganga
643 River and factors affecting their distributions. *Catena*, 204, 105360, 2021.

644 Ramaswamy, V., Gaye, B., Shirodkar, P.V., Rao, P.S., Chivas, A. R., Wheeler, D., and Thwin, S.: Distribution and
645 sources of organic carbon, nitrogen and their isotopic signatures in sediments from the Ayeyarwady (Irrawaddy)
646 continental shelf, northern Andaman Sea. *Mar. Chem.*, 111, 137-150, 2008.

647 Ramesh, R. and Sarin, M.M.: Stable isotope study of the Ganga (Ganges) river system. *J. Hydrology*, 139, 49-62,
648 1992.

649 Rao, R. R., and Sivakumar, R.: Seasonal variability of sea surface salinity and salt budget of the mixed layer of the
650 northIndian Ocean. *J. Geophys. Res.*, 108(C1), 3009, 2003.

651 Rixen, T., Cowie, G., Gaye, B., Goes, J., do Rosário Gomes, H., Hood, R.R., Lachkar, Z., Schmidt, H., Segsneider,
652 J., and Singh, A.: Reviews and syntheses: Present, past, and future of the oxygen minimum zone in the northern
653 Indian Ocean. *Biogeosciences*, 17, 6051-6080, 2020.

654 Rochford, D. J.: Salinity maximum in the upper 100 meters of the north Indian Ocean. *Aust. J. Mar. Freshwater Res.*,
655 15, 1-24, 1964.

656 [Rozanski, K., Araguás-Araguás, L., and Gonfiantini, R.: Isotopic Patterns in Modern Global Precipitation, in: *Climate
657 Change in Continental Isotopic Records*, edited by: Swart, P. K., Lohmann, K. C., Mckenzie, J., and Savin, S.,
658 American Geophysical Union, Washington, D. C., 1–36, <https://doi.org/10.1029/GM078p0001>, 1993.](#)

659 Saalim, S.M., Saraswat, R., and Nigam, R.: Ecological preferences of living benthic foraminifera from the Mahanadi
660 river-dominated north-western Bay of Bengal: A potential environmental impact assessment tool. *Mar. Poll. Bull.*,
661 175, 113158, 2022.

662 [Sánchez, A., Sánchez-Vargas, L., Balart, E., and Domínguez-Samalea, Y.: Stable oxygen isotopes in planktonic](#)
663 [foraminifera from surface sediments in the California Current system. *Mar. Micropaleontol.*, 173, 102127, 2022.](#)

664 Saraswat, R., Lea, D.W., Nigam, R., Mackensen, A., and Naik, D.K.: Deglaciation in the tropical Indian Ocean driven
665 by interplay between the regional monsoon and global teleconnections. *Earth Planet. Sci. Lett.*, 375, 166-175,
666 2013.

667 Saraswat, R., Nigam, R., Mackensen, A., and Weldeab, S.: Linkage between seasonal insolation gradient in the tropical
668 northern hemisphere and the sea surface salinity of the equatorial Indian Ocean during the last glacial period. *Acta*
669 *Geol. Sinica*, 86, 801–811, 2012.

670 Saraswat, R., Singh, D.P., Lea, D.W., Mackensen, A., and Naik, D.K.: Indonesian throughflow controlled the
671 westward extent of the Indo-Pacific Warm Pool during glacial-interglacial intervals. *Global Planet. Cha.*, 183,
672 103031, 2019.

673 Saraswat, R., Suokhrie, T., Naik, D.K., Singh, D.P., Saalim, S.M., Salman, M., Kumar, G., Bhadra, S.R., Mohtadi,
674 M., Kurtarkar, S.R., and Maurya, A.S.: Oxygen isotopic ratio of *Globigerinoides ruber* (white variety) in the
675 surface sediments of the northern Indian Ocean. PANGAEA, <https://doi.org/10.1594/PANGAEA.945401>, 2022.

676 [Sarma, V.V. and Aswanikumar, V.: Subsurface chlorophyll maxima in the north-western Bay of Bengal. *J. Plankton*](#)
677 [Res.](#), 11, 339-352, 1991.

678 Sarma, V.V.S.S., Chopra, M., Rao, D.N., Priya, M.M.R., Rajula, G.R., Lakshmi, D.S.R., and Rao, V.D.: Role of
679 eddies on controlling total and size-fractionated primary production in the Bay of Bengal. *Cont. Shelf Res.*, 204,
680 104186, 2020.

681 Schlitzer, R., Ocean Data View, <https://odv.awi.de>, 2018.

682 Schmidt, G.A., Bigg, G.R., and Rohling, E.J.: "Global Seawater Oxygen-18 Database - v1.22"
683 <https://data.giss.nasa.gov/o18data/>, 1999.

684 [Schmidt, M.W., Spero, H.J., and Lea, D.W.: Links between salinity variation in the Caribbean and North Atlantic](#)
685 [thermohaline circulation. *Nature*, 428, 160–163, 2004.](#)

686 Schrag, D.P., DePaolo, D.J., Richter, F.M.: Reconstructing past sea surface temperatures: Correcting for diagenesis
687 of bulk marine carbonate. *Geochim. Cosmochim. Acta*, 59, 2265–2278, 1995.

688 Sengupta, D., Bharath Raj, G.N., and Shenoi, S.S.C.: Surface freshwater from Bay of Bengal runoff and Indonesian
689 Throughflow in the tropical Indian Ocean. *Geophys. Res. Lett.*, 33, L22609, 2006.

690 Shackleton, N.J.: Oxygen isotopes, ice volume and sea level. *Quat. Sci. Rev.*, 6, 183-190, 1987.

691 Shackleton, N.J.: The 100,000-year Ice-Age cycle identified and found to lag temperature, carbon dioxide, and orbital
692 eccentricity. *Science*, 289, 1897-1902, 2000.

693 Shackleton, N.J., and Vincent, E.: Oxygen and carbon isotope studies in recent foraminifera from the southwest Indian
694 ocean. *Mar. Micropaleontol.*, 3, 1-13, 1978.

695 Shankar, D., Vinayachandran, P.N., and Unnikrishnan, A.S.: The monsoon currents in the north Indian Ocean. *Progr.*
696 *Oceanogra.*, 52, 63–120, 2002.

697 Shetye, S.R., Gouveia, A.D., and Shenoi, S.S.C.: Circulation and water masses of the Arabian Sea. *Proc. Indian Acad.*
698 *Sci. (Earth Planet. Sci.)*, 103, 107-123, 1994.

699 Shetye, S.R., Shenoi, S.S.C., Gouveia, A.D., Michael, G.S., Sundar, D., and Nampoothiri, G.: Wind-driven coastal
700 upwelling along the western boundary of the Bay of Bengal during the southwest monsoon. *Cont. Shelf Res.*, 11,
701 1397-1408, 1991.

702 Singh, A., Jani, R.A., and Ramesh, R.: Spatiotemporal variations of the $\delta^{18}\text{O}$ -salinity relation in the northern Indian
703 Ocean. *Deep-Sea Res. I*, 57, 1422-1431, 2010.

704 Singh, D.P., Saraswat, R., and Naik, D.K.: Does glacial-interglacial transition affect sediment accumulation in
705 monsoon dominated regions? *Acta Geol. Sinica*, 91, 1079-1094, 2017.

706 Singh, D.P., Saraswat, R., and Nigam, R.: Untangling the effect of organic matter and dissolved oxygen on living
707 benthic foraminifera in the southeastern Arabian Sea. *Mar. Poll. Bull.*, 172, 112883, 2021.

708 Sirocko, F.: Zur Akkumulation von Staubsedimenten im nördlichen Indischen Ozean; Anzeiger der Klimageschichte
709 Arabiens und Indiens. Dissertation, Berichte-Reports, Geologisch-Paläontologisches Institut der Universität Kiel,
710 27, 185 pp, 1989.

711 Smitha, A., Joseph, K.A., Jayaram, C., and Balchand, A.N.: Upwelling in the southeastern Arabian Sea as evidenced
712 by Ekman mass transport using wind observations from OCEANSAT-II Scatterometer. *Indian J. Geo-mar. Sci.*,
713 43, 111-116, 2014.

714 Spero, H.J., Bijma, J., Lea, D.W., and Bemis, B.B.: Effect of seawater carbonate concentration on foraminiferal carbon
715 and oxygen isotopes. *Nature*, 390, 497-500, 1997.

716 Sridevi, B., and Sarma, V.V.S.S.: A revisit to the regulation of oxygen minimum zone in the Bay of Bengal. *J. Earth
717 Syst. Sci.*, 129, 1-7, 2020.

718 Stainbank, S., Kroon, D., Rüggeberg, A., Raddatz, J., de Leau, E.S., Zhang, M., et al.: Controls on planktonic
719 foraminifera apparent calcification depths for the northern equatorial Indian Ocean. *PLoS ONE* 14, e0222299,
720 2019.

721 Suokhrie, T., Saraswat, R., and Nigam, R.: Multiple ecological parameters affect living benthic foraminifera in the
722 river-influenced west-central Bay of Bengal. *Front. Mar. Sci.*, 8, 467, 2021a.

723 Suokhrie, T., Saraswat, and R., Saju, S.: Strong solar influence on multi-decadal periodic productivity changes in the
724 central-western Bay of Bengal. *Quat. Int.*, <https://doi.org/10.1016/j.quaint.2021.04.015>, 2021b.

725 Thirumalai, K., Richey, J.N., Quinn, T.M., and Poore, R.Z.: *Globigerinoides ruber* morphotypes in the Gulf of
726 Mexico: A test of null hypothesis. *Sci. Rep.*, 4, 6018, 2014.

727 Thompson, P.R., Bé, A.W.H., Duplessy, J.-C., and Shackleton, N.J.: Disappearance of pink-pigmented
728 *Globigerinoides ruber* at 120,000 yr BP in the Indian and Pacific oceans. *Nature*, 280, 554-558, 1979.

729 Thunell, R., Tappa, E., Pride, C., and Kincaid, E.: Sea-surface temperature anomalies associated with the 1997-1998
730 El Niño recorded in the oxygen isotope composition of planktonic foraminifera. *Geology*, 27, 843,
731 [https://doi.org/10.1130/0091-7613\(1999\)027<0843:SSTA AW>2.3.CO;2](https://doi.org/10.1130/0091-7613(1999)027<0843:SSTA AW>2.3.CO;2), 1999.

732 Tiwari, M., Nagoji, S.S., Kartik, T., Drishya, G., Parvathy, R.K., and Rajan, S.: Oxygen isotope-salinity relationships
733 of discrete oceanic regions from India to Antarctica vis-à-vis surface hydrological processes. *J. Mar. Syst.*, 113-
734 114, 88-93, 2013.

735 Urey, H.C.: The thermodynamic properties of isotopic substances. *J. Chem. Soc.*, 12, 562-569, 1947.

736 Vergnaud-Grazzini, C.: Non-equilibrium isotopic compositions of shells of planktonic foraminifera in the
737 Mediterranean Sea. *Palaeogeogra., Palaeoclimatol., Palaeoecol.*, 20, 263-276, 1976.

738 Vinayachandran, P.N., and Shetye, S.R.: The warm pool in the Indian Ocean. *Proc. Indian Acad. Sci. (Earth Planet*
739 *Sci.)* 100, 165-175, 1991.

740 Waelbroeck, C., Mulitza, S., Spero, H., Dokken, T., Kiefer, T., and Cortijo, E.: A global compilation of late Holocene
741 planktonic foraminiferal $\delta^{18}\text{O}$: relationship between surface water temperature and $\delta^{18}\text{O}$. *Quat. Sci. Rev.*, 24, 853–
742 868, <https://doi.org/10.1016/j.quascirev.2003.10.014>, 2005.

743 Wang, L., Sarnthein, M., Duplessy, J.-C., Erlenkeuser, H., Jung, S., and Pflaumann, U.: Paleo sea surface salinities in
744 the low-latitude Atlantic: The $\delta^{18}\text{O}$ record of *Globigerinoides ruber* (white). *Paleoceanography*, 10, 749-761, 1995.

745 Wu, G., and Berger, W.H.: Planktonic foraminifera: differential dissolution and the quaternary stable isotope record
746 in the west equatorial Pacific. *Paleoceanography*, 4, 181-198, 1989.

747 Wycech, J.B., Kelly, D.C., Kitajima, K., Kozdon, R., Orland, I.J., and Valley, J.W.: Combined effects of gametogenic
748 calcification and dissolution on $\delta^{18}\text{O}$ measurements of the planktic foraminifer *Trilobatus sacculifer*. *Geochem.*
749 *Geophys. Geosys.*, 19, <https://doi.org/10.1029/2018GC007908>, 2018.

750 Zweng, M M., Reagan, J. R., Seidov, D., Boyer, T. P., Locarnini, R. A., Garcia, H. E., Mishonov, A. V., Baranova,
751 O. K., Weathers, K., Paver, C. R. and Smolyar, I.: World Ocean Atlas 2018, Volume 2: Salinity. A. Mishonov
752 Technical Ed.; NOAA Atlas NESDIS 82, 50pp, 2018.